A Dynamic Model of Excitation-Contraction Coupling during Acidosis in Cardiac Ventricular Myocytes

Edmund J. Crampin and Nicolas P. Smith
Bioengineering Institute and Department of Engineering Science, University of Auckland, Auckland, New Zealand

ABSTRACT Acidosis in cardiac myocytes is a major factor in the reduced inotropy that occurs in the ischemic heart. During acidosis, diastolic calcium concentration and the amplitude of the calcium transient increase, while the strength of contraction decreases. This has been attributed to the inhibition by protons of calcium uptake and release by the sarcoplasmic reticulum, to a rise of intracellular sodium caused by activation of sodium-hydrogen exchange, decreased calcium binding affinity to Troponin-C, and direct effects on the contractile machinery. The relative contributions and concerted action of these effects are, however, difficult to establish experimentally. We have developed a mathematical model to examine altered calcium-handling mechanisms during acidosis. Each of the alterations was incorporated into a dynamical model of pH regulation and excitation-contraction coupling to predict the time courses of key ionic species during acidosis, in particular intracellular pH, sodium and the calcium transient, and contraction. This modeling study suggests that the most significant effects are elevated sodium, inhibition of sodium-calcium exchange, and the direct interaction of protons with the contractile machinery; and shows how the experimental data on these contributions can be reconciled to understand the overall effects of acidosis in the beating heart.

INTRODUCTION

Acidosis is a major factor underlying the damage that occurs as a result of disrupted blood supply during coronary heart disease. Reduced intracellular pH disrupts each of the steps in excitation-contraction coupling, and severely affects the ability of the myocyte to generate tension, with dire consequences for the pumping capacity of the heart. Considerable experimental data exists on the effects of acidosis on different processes in cardiac myocytes. Typically, in these studies respiratory acidosis is induced by raising extracellular CO_2, which causes intracellular pH to fall.

Despite the important implications of acidosis, the relative significance of the various mechanisms by which decreased intracellular pH affects the steps of excitation-contraction coupling and force generation remain under debate. This is largely due to two factors that make data difficult to interpret unambiguously. First is the manner in which pH, ionic concentrations, and developed tension vary with time during acidosis. For example, when acidosis is induced by increasing extracellular CO_2 concentration, tension shows a biphasic response, with an initial rapid decline followed by a slower partial recovery (see Fig. 1). This response is due to the competing effects of acidosis on cellular processes involved in calcium handling, as well as direct effects on the contractile proteins. Secondly, the effects of acidosis on intracellular Ca^{2+} and tension are the result of the interactions between multiple coupled cellular processes, each with its own nonlinear dependencies and intrinsic timescale.

In the heart, contraction is first signaled by depolarization of the cell membrane. This causes voltage-dependent L-type Ca^{2+} channels to open and a local increase in Ca^{2+} concentration adjacent to the Ca^{2+} release channels (ryanodine receptors, RyRs) of the sarcoplasmic reticulum (SR). The local release causes the RyRs to open, producing a much larger efflux of calcium from the SR into the cytosol. The raised Ca^{2+} concentration increases the proportion of regulatory sites on the protein Troponin-C (TnC) to which Ca^{2+} is bound. Binding of Ca^{2+} to TnC induces a conformational change in the contractile proteins allowing actin and myosin to bind, forming cross-bridges that develop tension. Ca^{2+} concentration is then returned to diastolic level via time-dependent closing of the RyRs, Ca^{2+} uptake into the SR by the SR Ca^{2+}-pump (SERCA), and Ca^{2+} efflux from the cell via the sarcolemmal Ca^{2+}-pump and Na^{+}-Ca^{2+} exchanger (NCX).

The cytosolic Ca^{2+} transients that initiate contraction are strongly sensitive to pH. Studies have found consistently that acidosis raises diastolic Ca^{2+} (1) and decreases the rate of decline of the calcium transient (2). Systolic Ca^{2+}, however, has been shown to increase (2,3) or show no change (4) during acidosis (or, in voltage-clamped myocytes, even to decrease (5)). The mechanisms by which these changes are effected and the reasons for the discrepancies are not completely clear. Acidosis inhibits most, if not all, of the steps in excitation-contraction coupling outlined above. Calcium release from the SR was found by Kentish and Xiang (6) to be reduced by >50% when pH was lowered to 6.5, attributed at least in part to competitive binding of protons at cytosolic Ca^{2+} activation sites. Moreover, fractional SR release decreases as pH is lowered. Therefore, it appears contrary that

Submitted July 12, 2005, and accepted for publication January 23, 2006.

Edmund J. Crampin and Nicolas P. Smith contributed equally to this article.

Address reprint requests to Edmund J. Crampin, Bioengineering Institute, University of Auckland, Private Bag 92019, Auckland, New Zealand. Tel.: 64-9-373-7599 ext. 88168; E-mail: e.crampin@auckland.ac.nz.

0006-3495/06/05/3074/17 $2.00

doi: 10.1529/biophysj.105.070557

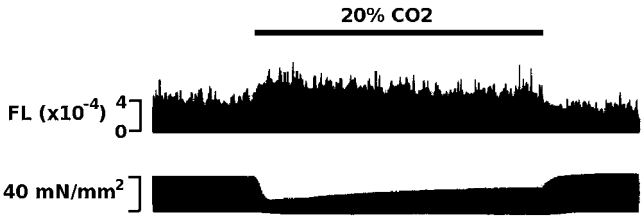

FIGURE 1 The effect of acidosis on intracellular Ca^{2+} and contractile force in rat papillary muscle, reproduced from Orchard et al. (57). Intracellular calcium (as indicated by photoprotein aquorin light intensity; *top*) and developed tension (*bottom*) during respiratory acidosis induced by raising CO_2 from 5% to 20% with HCO_3^- held constant. (Reproduced from The Journal of General Physiology, 1987, 90:145–165 by copyright permission of the Rockefeller University Press.)

peak systolic calcium concentration may actually rise during acidosis despite depressed Ca^{2+} release.

There are, however, established mechanisms that contribute to an increase in cytosolic Ca^{2+}. Protons displace Ca^{2+} from TnC binding sites, reducing Ca^{2+} buffering within the cell. Diastolic calcium concentration increases in acidosis, which under normal circumstances would lead to increased SR loading via calcium uptake by the SR Ca^{2+}-pump—potentially a mechanism to increase the size of the transient. SERCA is, however, directly inhibited by protons; the slowed uptake of calcium into the SR is thought to underlie the marked slowing in the decline of the transient (6). Yet many studies have found that SR calcium content increases during acidosis (4,7), although others have reported a decrease (6). Pathways for Ca^{2+} removal from the cytosol are also inhibited at low pH, which would increase the amount of Ca^{2+} in the cell. Na^+-Ca^{2+} exchange is directly inhibited by protons (8–10); however, during acidosis intracellular Na^+ rises, due to Na^+-coupled extrusion of protons. This decreases Na^+-coupled Ca^{2+} efflux, which further contributes to rising cytosolic Ca^{2+}. Bountra and Vaughan-Jones (11) showed that this inotropic effect can at least partially compensate for the direct inhibitory effects of lowered intracellular pH.

Finally, acidic pH has also been shown to affect the Ca^{2+}-tension curve (12). Acidosis decreases the apparent sensitivity of the regulatory sites of TnC to Ca^{2+}, shifting the activation curve to higher Ca^{2+} with little change in its shape and slope. This effect arises from direct competition for the low affinity binding sites of TnC (2,13). Additionally, a drop in pH decreases the maximum (Ca^{2+}-saturating) tension, producing a 30% reduction at pH 6.5 (2).

The intracellular environment is highly regulated, and intracellular pH is no exception. Cellular proton concentration is strongly buffered, approximately equally by CO_2-dependent and CO_2-independent intrinsic buffers under normal conditions. pH is also regulated by four sarcolemmal transporters: sodium-bicarbonate co-transport (NBC) and sodium-hydrogen exchange (NHE) are acid extruders increasing intracellular pH, while chloride-hydroxide exchange (CHE) and bicarbonate-chloride exchange (anion exchanger, AE) are acid loaders.

In this study, we describe the development of a dynamic model of acidosis in the ventricular myocyte. Mathematical modeling provides a mechanism by which the effects of individual mechanisms can be isolated, and their significance quantified, to further our understanding of the effects of acidosis on the myocyte.

The model incorporates experimental data on pH-dependent changes to calcium-handling and buffering, and acid transport process into a coupled modeling framework for cell electrophysiology (14) and mechanics (15). Our strategy for examining the contributions of the changes to excitation-contraction coupling that occur during acidosis is to quantify the influence on the calcium transient of each mechanism in turn, before examining their collective effects on the cell. This approach is made possible with a modeling, rather than an experimental study; however, it is important to note at the outset that, for a highly coupled nonlinear system such as this, the combined effects of these mechanisms will differ from the sum of changes engendered by each mechanism individually. Nevertheless, many useful insights can be gained. We use the model to examine the effects of acidosis on each of the steps in excitation-contraction coupling over multiple beats. In particular, we focus on the dynamical changes underlying the biphasic nature of the reduced inotropy brought about by respiratory acidosis, and we seek to rationalize the discrepancies apparent in the literature regarding the effects of acidosis on SR Ca^{2+} content and release. This study develops and extends the preliminary work recently presented by Crampin et al. (16) to a dynamical modeling framework.

METHODS

We base our analysis on the Luo-Rudy-dynamic (LRd) model of myocyte electrophysiology (14,17), as that model 1), is based on Guinea-pig electrophysiology which is consistent with the majority of acid transport data; and 2), has the properties required to maintain stable voltage and ionic concentrations over multiple action potentials. Our implementation of the model follows Hund et al. (18), with modifications as described below and in the Appendix. A schematic of the model is shown in Fig. 2.

SR calcium release channels

Single channel recordings on purified channel preparations provide detailed data on which to base a quantitative description of this inhibition. These experiments, reported by Rousseau and Pinkos (19) and Xu et al. (20), showed that single-channel open probability decreases with increasing cytosolic acidosis, while Xu et al (20) also found that single-channel conductance was not changed—i.e., the inhibition is due to lowered Ca^{2+} sensitivity of the RyRs with falling pH. The mechanism for this shift is a reduction in the apparent affinity for Ca^{2+} at high affinity calcium-activation sites (20). These latter experiments, on canine cardiac release channels, show the Ca^{2+}-dependence of the open channel probability, P_0 which is maximally activated at $P_0 \sim 0.7$ for $[Ca^{2+}]_i \sim 0.1$ mM, is inhibited at higher intracellular calcium. When $[Ca^{2+}]$ is held constant, P_0 falls toward zero as pH decreases below ~6.

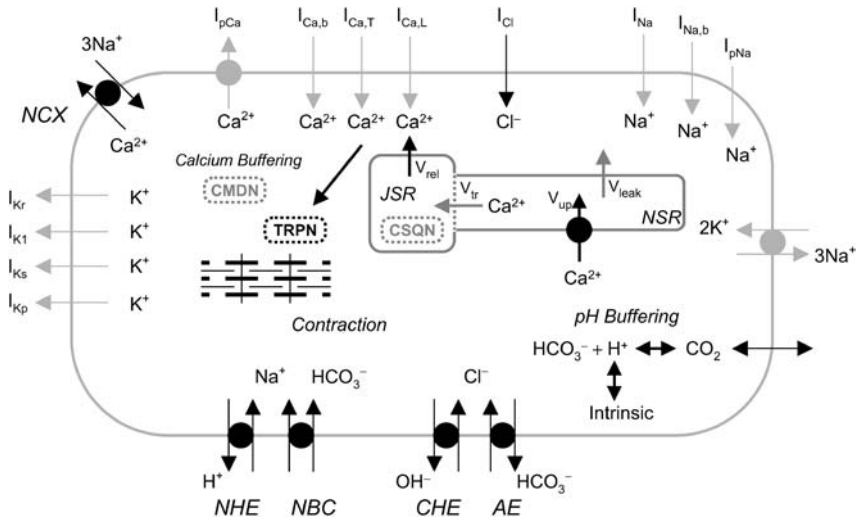

FIGURE 2 Schematic diagram of the model. Existing model components of the LRd model are shown in shading, whereas additions to the model and modified components (mechanisms regulated by pH) are shown in solid representation. Abbreviations: *NCX*, sodium-calcium exchanger. Acid efflux pathways: *NHE*, sodium-hydrogen exchanger and *NBC*, Na-bicarbonate cotransporter. Acid influx pathways: *CHE*, chloride-hydroxide exchanger and *AE*, anion exchanger. *CMDN*, calmodulin; *TRPN*, troponin C; *CSQN*, calsequestrin; *JSR*, junctional SR; and *NSR*, network SR.

Experiments in which cytosolic and SR lumenal pH were varied independently showed that the cytosolic pH is the dominant effector. As the SR is permeable to protons, we have used these data to model the inhibition. The LRd ventricular cell model does not explicitly model the kinetics of RyRs. Assuming the maximal channel conductance g_{maxrel} is proportional to the open channel probability, we have modified the calcium release flux to include a simple saturating inhibition, using data on the dependence of single channel open probability on pH from Xu et al. (20),

$$P_0 = \frac{P_0^{\infty}}{1 + 10^{n_{\mathrm{rel}}(-\mathrm{pH}+\mathrm{pK}_{\mathrm{rel}})}}, \tag{1}$$

shown in Fig. 3 *a*, so that the pH-dependence of the conductance is given by $g_{\mathrm{maxrel}}P_0/P_0^{\infty}$. Examination of Ca^{2+} transients in the LRd model shows that, with the published parameter set, the junctional compartment empties completely with each beat, thus the magnitude of Ca^{2+} release for each beat is determined by the filling fraction of this compartment, rather than the characteristics of the release channel. Under such a scenario, inhibition of the release mechanism will have no effect on the Ca^{2+} transient until the inhibition is severe enough that this, rather than the amount of Ca^{2+} available for release, becomes the limiting factor. Therefore we have also decreased the maximal release channel conductance by a factor of 4, so that the Ca^{2+} released is sensitive to the channel conductance, but does not change Ca^{2+} transients in the model at normal pH. Parameters are given in Table 1.

SR calcium pump

Several studies have reported direct inhibition by protons of calcium uptake into the SR (2,12,21). The steady-state Ca^{2+}-ATPase activity and calcium transport show bell-shaped dependence on pH, with peak activity at pH ~ 7–8 (22,23), with calcium uptake into the SR progressively reduced at more acidic pH. This pH sensitivity has been associated with at least two states of the protein: the formation of the phospho-enzyme (24) and the calcium binding state (21).

Henderson et al. (25) reported equilibrium fluorescence studies on skeletal Ca^{2+}-ATPase, which reveal sigmoidal intensity variation, increasing at higher pH. These and similar data have been interpreted as pH dependence of the conformational change between cytosol-facing and SR lumen-facing states of the protein, due to ATP binding and covalent phosphorylation (24,26). To produce a simplified model of pH inhibition of SR calcium uptake we have fitted these equilibrium data, assuming that the fluorescence change indicates a transition from an active, Ca^{2+}-binding state to an inactive state of the transporter:

$$J_{\mathrm{up}} = \frac{J_{\mathrm{up}}^{\infty}}{1 + 10^{n_{\mathrm{up}}(-\mathrm{pH}+\mathrm{pK}_{\mathrm{up}})}}\left(\frac{[Ca^{2+}]_i}{[Ca^{2+}]_i + K_{\mathrm{M,up}}}\right). \tag{2}$$

The pH-dependence of this flux is shown in Fig. 3 *b*, with parameters given in Table 1.

Na^+-Ca^{2+} exchanger

Doering and Lederer (10,27) measured Na^+-Ca^{2+} exchange current in giant excised patches from Guinea-pig ventricular myocytes under different cytosolic acid loading conditions, and reported a biphasic inhibition of the current after a step change in pH with a rapid initial block followed by a slower secondary phase. They also showed that proton sensitivity is abolished by the action of a protease, which leaves the exchanger functionally intact, therefore suggesting that protons interact with the exchanger at a location away from the transport site. Recent data from Egger and Niggli (28) found that the Na^+-Ca^{2+} exchanger is also inhibited by extracellular acid, reducing the exchanger current to ~70% of normal peak values at pH_e 6. As this reduction in current is ~10% of the inhibitory effect of a similar fall in intracellular pH, it has not been included in the model.

We have modeled inhibition of the Na^+-Ca^{2+} exchanger assuming that proton binding at a regulatory site affects each state of the transport cycle equally, fitting data from Doering and Lederer (27) showing the change in steady-state outward exchanger current at different pH_i (see Fig. 3 *c*). The pH-dependence of the current at constant ligand concentrations is

$$I_{\mathrm{NaCa}} \propto \frac{1 + 10^{n_{\mathrm{NaCa}}(-\mathrm{pH}_{\mathrm{ref}}+\mathrm{pK}_{\mathrm{NaCa}})}}{1 + 10^{n_{\mathrm{NaCa}}(-\mathrm{pH}+\mathrm{pK}_{\mathrm{NaCa}})}}, \tag{3}$$

where pH_{ref} is a reference pH value, with parameters given in Table 1.

L-type Ca^{2+} current

Hulme and Orchard (1998) report that, under physiological conditions, the L-type Ca^{2+} current, I_{CaL}, is unchanged during acidosis; older studies, however, where intracellular Ca^{2+} was held constant (buffered), found I_{CaL} to be substantially inhibited. Under physiological conditions, $[Ca^{2+}]_i$ rises during acidosis, and this increases the activity of Ca^{2+}-calmodulin-dependent protein kinase II (CaMKII), which activates I_{CaL}—potentially offsetting any inhibition due to H^+ inhibition (29). Therefore, on the basis of these more recent data, we have not changed I_{CaL} due to acidosis in the model.

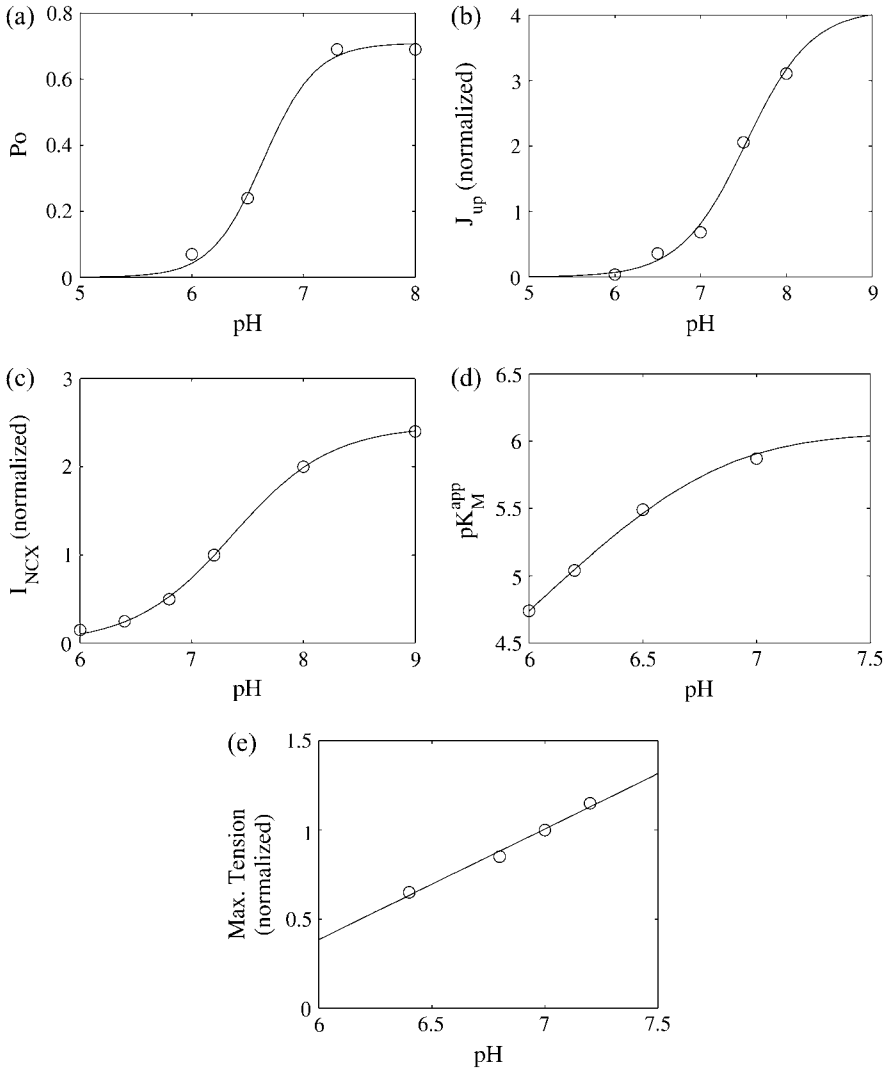

FIGURE 3 (*a*) pH dependence of RyR open probability, data (○) from Xu et al. (20); measurements at 10 μM Ca^{2+}, maximal open probability taken as 0.7. (*b*) pH dependence of Ca^{2+} uptake flux into the SR at constant $[Ca^{2+}]_i$, fitted from normalized fluorescence data (○) from Henderson et al. (25) (at 10 mM Mg^{2+}). (*c*) Proton inhibition of NCX flux, data (○) from Doering and Lederer (27). (*d*) pH-dependence of Troponin-Ca^{2+} affinity, half-maximal activation curve fitted to data (○) from Blanchard and Solaro (13). (*e*) pH-dependence of maximum tension, data (○) from Orchard and Kentish (2). Parameters for each of these fits are in Table 1.

Modeling tension

Developed tension is calculated assuming isometric contraction at a sarcomere length of 2 μm using a steady-state version of the model by Hunter et al. (15). This model has two components: 1), the calcium transient and calcium binding to the thin filaments; and 2), the availability of thin-filament binding sites. At a constant extension ratio, the amount of calcium bound to the Troponin-C is a saturating function,

$$[\mathrm{Ca}]_{\mathrm{trpn}} = \frac{[\overline{\mathrm{TRPN}}][\mathrm{Ca}^{2+}]_i}{K_{\mathrm{M,trpn}}^{\mathrm{app}} + [\mathrm{Ca}^{2+}]_i}, \tag{4}$$

where $[\overline{\mathrm{TRPN}}]$ is the total cellular concentration of available binding sites, as defined in the LRd model, and $K_{\mathrm{M,trpn}}^{\mathrm{app}}$ is the apparent binding constant for Ca^{2+}.

As a result of calcium binding to Troponin-C, a conformational change in the contractile proteins occurs, making thin-filament binding sites available. The kinetics of this process are governed by the first-order equation for the fraction of available sites z,

$$\frac{\mathrm{d}z}{\mathrm{d}t} = \alpha_0 \left(\left(\frac{[\mathrm{Ca}^{2+}]_{\mathrm{trpn}}}{C_{50}} \right)^{n_z} (1-z) - z \right), \tag{5}$$

and the tension developed at steady state is proportional to the number of available binding sites,

$$T = T_{\max} z, \tag{6}$$

so that $T(z = 0) = 0$, and $T_{\max}$ is the maximum tension.

Blanchard and Solaro (13) measured the amount of Ca^{2+} bound to Troponin and determined that there is a reduction in the affinity of myofibrillar Troponin-C for calcium with acidic pH, which is responsible for the reduction in tension. We have used these data to calculate an apparent K_M for competitive binding of protons at the low affinity Ca^{2+} binding sites, Fig. 3 *d*. The apparent binding constant is given by

$$K_{\mathrm{M,trpn}}^{\mathrm{app}} = K_{\mathrm{M,trpn}} \left(\frac{1 + 10^{n_{\mathrm{trpn}}(-\mathrm{pH}+\mathrm{pK}_{\mathrm{trpn}})}}{1 + 10^{n_{\mathrm{trpn}}(-\mathrm{pH}_{\mathrm{ref}}+\mathrm{pK}_{\mathrm{trpn}})}} \right), \tag{7}$$

where the LRd model value was used for $K_{\mathrm{M,trpn}}$.

The Blanchard and Solaro (13) study on intact myofibrils reported no change in maximum tension generated (for saturating Ca^{2+}). Studies on skinned fibers have, however, shown a marked decrease in maximum force during acidosis (2). Furthermore, there is evidence of reduced maximal Ca^{2+}-activated force (developed pressure) with falling pH in intact hearts (30), and, more recently, in intact papillary muscle preparations (31).

TABLE 1 Fitted parameters describing pH-dependence in the myocyte

Description	Units	Symbol	Value
RyR proton dissociation constant		pK_{rel}	6.64
RyR Hill coefficient		n_{rel}	1.87
RyR maximal open probability		P_0^{∞}	0.71
RyR maximum release rate constant	ms^{-1}	g_{maxrel}	7.5
SERCA proton dissociation constant		pK_{up}	7.53
SERCA Hill coefficient		n_{up}	1.14
SERCA maximal uptake flux	mM ms^{-1}	J_{up}^{∞}	0.036
NCX proton dissociation constant		pK_{NaCa}	7.37
NCX Hill coefficient		n_{NaCa}	0.991
TRPN proton dissociation constant		pK_{trpn}	6.79
TRPN Hill coefficient		n_{trpn}	1.65
TRPN total cell concentration	mM	$[\overline{TRPN}]$	0.07
Thin-filament Hill activation parameter	mM	C_{50}	0.06
Thin-filament Hill coefficient		n_z	8.0
Thin-filament rate constant	ms^{-1}	α_0	0.2
Maximum tension-pH dependence		b_T	0.621
Reference (normal) pH		pH_{ref}	7.15

Evidence is now accumulating that the thin-filament protein Troponin I (TnI) is also regulated by pH (32). We have included this effect as a simple empirical fit to data from Orchard and Kentish (2), to find the dependence of maximum tension on pH, Fig. 3 *e*,

$$T_{max} = T_{ref}(1 + b_T(pH - pH_{ref})), \tag{8}$$

where T_{ref} is the maximal tension obtained at the reference pH.

The Ca^{2+}-tension curves corresponding to these equations are plotted in Fig. 4, which correspond well to experimental curves measured by Orchard and Kentish (2).

Modeling pH regulation

Model components describing the regulation and transport of protons, required to determine the time course of pH and associated ionic changes, are described below, adapted from Boron and Weer (33) and Leem and Vaughan-Jones (34). Protons are strongly buffered in the myocyte, by CO_2-dependent and CO_2-independent mechanisms. The extent of buffering is itself dependent on intracellular pH, and is quantified by the buffering power, β, which measures the instantaneous change in proton concentration required for a drop in pH of one unit. The CO_2-independent intrinsic buffering is thought to be due to protons binding to histidine residues, and to ATP and Pi (35). Intrinsic buffering power falls as pH rises over the physiological range (from 50 mM/pH unit at pH 6 to ~20 mM/pH unit at pH 7.6) and comprises at least two distinct buffers, here B_1 and B_2 (35),

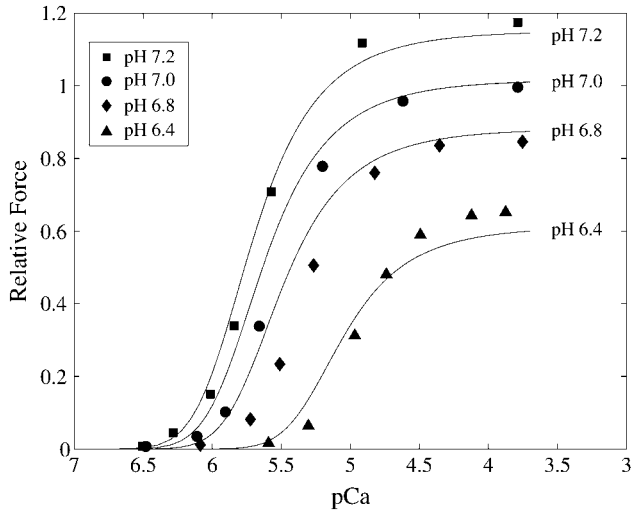

FIGURE 4 Steady-state pCa-tension curves normalized to maximum tension at pH 7, compared to experimental data points from Fig. 4 in Orchard and Kentish (2).

$$\beta_i(pH_i) = \ln 10\left(10^{(-pH_i)} + \frac{10^{(pK_1-pH_i)}[B_1]}{(1+10^{(pK_1-pH_i)})^2} + \frac{10^{(pK_2-pH_i)}[B_2]}{(1+10^{(pK_2-pH_i)})^2}\right) \tag{9}$$

(in the absence of buffers, $[B_1] = [B_2] = 0$, the resultant term in Eq. 9 reflects the translation from flux of $[H^+]$ to rate of pH change). CO_2-dependent buffering is via the CO_2 hydration reaction,

$$CO_2 + H_2O \underset{k_{hyd}^-}{\overset{k_{hyd}^+}{\rightleftharpoons}} HCO_3^- + H^+, \tag{10}$$

for which buffering power increases with increasing pH (from ~15 mM/pH unit at pH 6.9 to ~50 mM/pH unit at pH 7.3; (35)). This reaction is relatively slow, and is modeled as a flux according to

$$J_{hyd} = k_{hyd}^+[CO_2]_i - k_{hyd}^- 10^{-pH_i}[HCO_3^-]_i. \tag{11}$$

Parameters for Eqs. 9 and 11 were taken from Leem et al. (35), reproduced in Table 2.

The intracellular pH is then determined by

$$\frac{dpH}{dt} = -\frac{1}{\beta_i}(J_{che} - J_{nhe} + J_{hyd}), \tag{12}$$

where J_{nhe} and J_{che} are fluxes for the transporters NHE and CHE, respectively. Assuming the sarcolemma is permeable to CO_2 and impermeable to bicarbonate, transport of bicarbonate and CO_2 are given by

TABLE 2 Parameters for intrinsic and CO_2-dependent proton buffering, from Leem et al. (35)

Description	Units	Symbol	Value
Total concentration, intrinsic buffer species 1	mM	$[B_1]$	84.2
Dissociation constant, intrinsic buffer species 1		pK_1	6.03
Total concentration, intrinsic buffer species 2	mM	$[B_2]$	29.4
Dissociation constant, intrinsic buffer species 2		pK_2	7.57
Membrane permeability to CO_2	cm ms^{-1}	p_{CO2}	0.197×10^{-3}*
CO_2 hydration forward rate constant	ms^{-1}	k_{hyd}^+	0.365×10^{-3}
CO_2 hydration backward rate constant	ms^{-1}	k_{hyd}^-	0.48×10^3

*Value modified from Leem et al. (35) to account for cell membrane area/volume ratio for LRd model.

$$\frac{d[CO_2]_i}{dt} = J_{CO_2} - J_{hyd}, \quad (13)$$

$$\frac{d[HCO_3^-]_i}{dt} = J_{hyd} + J_{nbc} - J_{ae}, \quad (14)$$

where J_{nbc} and J_{ae} are the NBC and AE fluxes, and J_{CO2} is the diffusive flux of CO_2 across the membrane

$$J_{CO_2} = p_{CO_2}\frac{A_m}{V_{myo}}([CO_2]_e - [CO_2]_i). \quad (15)$$

Here, p_{CO2} is the CO_2 permeability of the cell membrane, A_m is the membrane area, and V_{myo} is the myocyte volume.

The CO_2 hydration reaction is the mechanism by which varying extracellular CO_2 brings about a change in intracellular pH, which is how respiratory acidosis (acidosis arising from increased extracellular CO_2) occurs. CO_2 readily diffuses through the cell membrane (Eq. 15). Thus, increasing extracellular CO_2 causes an influx of CO_2 into the cell, which disequilibrates the CO_2-bicarbonate reaction. As the reaction reestablishes equilibrium, some of this intracellular CO_2 combines with water to form bicarbonate, releasing a proton, causing the rapid drop in pH_i. In our simulations of respiratory acidosis, we assume that extracellular bicarbonate does not change, and so extracellular pH also falls in response to the change in CO_2, so that the CO_2-bicarbonate equilibrium is maintained outside the cell.

Acid transporters

The experimental data available on the pH-dependence of the four sarcolemmal acid-equivalent fluxes are sufficient to model the transporters using six-state thermodynamic cycles. This explicitly represents ion-binding and transitions between intra- and extracellular conformational states of the transporters, and allosteric regulation of the transport fluxes by protons, at intracellular and extracellular binding sites, according to available pH_i and pH_e data. We employed a model reduction approach, following Smith and Crampin (36), made on the basis of rapid binding approximations, to produce simplified kinetic models for the transporters. Details can be found in the Appendix.

Na^+-HCO_3^- cotransporter (NBC)

While both electrogenic (NBCe-1-B) and electro-neutral (NBCn-1) isoforms of the Na^+-HCO_3^- cotransporter have been identified in the heart, the electroneutral NBCn-1 has been shown to be the dominant form in Guinea-pig ventricular myocytes (37) and so we have assumed an electroneutral 1:1 stoichiometry for NBC. We have assumed sequential ligand binding on the cotransporter at the extracellular side to be in the order of Na^+ followed by HCO_3^-.

Additional allosteric regulation occurs via proton binding to either intracellular or extracellular sites. Data from Vaughan-Jones and Spitzer (38) suggest that NBC is stimulated via intracellular proton binding at an allosteric site. In contrast, extracellular proton concentration was shown to inhibit NBC (39). The binding kinetics of these allosteric regulatory sites are assumed to be independent of the state of the transporter and have been modeled using a fully cooperative Hill expression and hence the steady-state flux for NBC is given by

$$J_{nbc} = \frac{J_{cotrans}(Na^+, HCO_3^-)}{(1 + 10^{n_i(pH_i - pK_i)})(1 + 10^{-n_e(pH_e - pK_e)})}, \quad (16)$$

where $J_{cotrans}$ is the flux through a generic compulsory-order sequential cotransporter, and is defined in the Appendix.

Na^+-H^+ exchanger (NHE)

NHE is the major pathway for acid efflux from the cell. We have modeled the NHE1 isoform of the transporter, found in cardiac tissue, assuming Na^+ must be released from the intracellular site before H^+ binds to the transporter. Data from Vaughan-Jones and Spitzer (38) suggest that acid extrusion on NHE is stimulated via protons binding at a regulatory intracellular allosteric binding site. This allosteric regulatory site is assumed to be independent of the state of the transporter and has been modeled using a fully cooperative Hill expression. Na^+ influx on NHE is found to be slowed if pH_e is low, as during ischemia (11). Vaughan-Jones and Spitzer (38) also proposed allosteric regulation of NHE at an extracellular site, although with a significantly weaker dependence than the intracellular site (with a Hill coefficient of 1 at the extracellular site, compared to ~3 at the intracellular site).

We have found that the dependence of the basic transport cycle flux on proton (ligand) binding at low extracellular pH is sufficient to fit existing experimental data (38,40), and thus no allosteric regulation of NHE by extracellular protons was included in the model. The steady-state flux is then

$$J_{nhe} = \frac{J_{exch}(H^+, Na^+)}{1 + 10^{n_i(pH_i - pK_i)}}, \quad (17)$$

where the generic compulsory-order sequential exchange flux J_{exch} is defined in the Appendix.

Cl^--OH^- exchanger (CHE)

There is little direct evidence for allosteric regulation, or otherwise, of acid extrusion on CHE—thus, no allosteric regulation of CHE was included in the model. The transmembrane Cl^--OH^- exchange flux is given by

$$J_{che} = J_{exch}(OH^-, Cl^-). \quad (18)$$

Anion exchanger (AE)

Although there is little direct evidence for allosteric regulation of the anion exchanger, to maintain the reported steady-state relationship between pH_i and pH_e over a range of extracellular pH values (38), we have found that intra- and extracellular regulation of AE was required, where the exchanger is inhibited at low intracellular pH and stimulated by extracellular protons, giving

$$J_{ae} = \frac{J_{exch}(HCO_3^-, Cl^-)}{(1 + 10^{-n_i(pH_i - pK_i)})(1 + 10^{n_e(pH_e - pK_e)})}. \quad (19)$$

Parameter estimation

We estimated parameters for these fluxes using a sequential quadratic programming algorithm (41) to optimize the model fit to pH_i-dependence data, measured by Leem et al. (35), and whole-cell steady-state pH_i and pH_e measurements (38,42). This approach allows multiple data sources to be used to constrain the model parameters. Additional data sources used were pH_e values required to reduce the NBC and NHE fluxes to zero (40), dependence of NBC flux on extracellular Na^+ (39), and estimates of intra- and extracellular Cl^- concentrations (43). Full details of the procedure employed are given in the accompanying Supplementary Material. Fitted flux curves and experimental data on pH_i-dependence for the transporters are shown in Fig. 5, and parameters are given in Table 3.

Simulation protocol

We simulated the LRd model, as described in Hund et al. (18), with the additions and modifications listed in Eqs. 1–19 and in the Appendix. The model is implemented using charge balance (44) to calculate the membrane potential, described in the Appendix. In all simulations, the cell is paced with a period of 500 ms for 10 min to achieve steady beat-to-beat cycles before inducing respiratory acidosis. (Values for initial conditions after pacing to

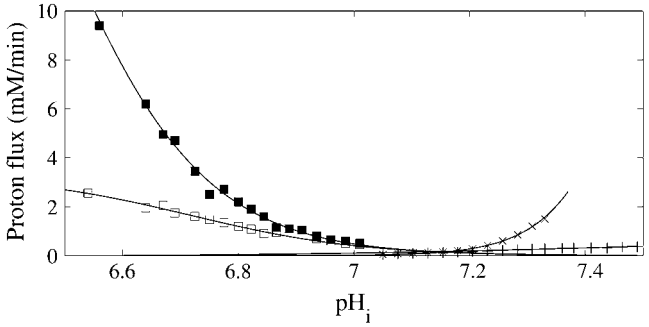

FIGURE 5 pH-dependence of sarcolemmal acid-equivalent transporters. Model fits (*solid lines*) and experimentally measured fluxes (35) showing ■ NBC, □ NHE, + CHE, and × AE.

steady-state cycles are provided in the Supplementary Material accompanying this article.) Charge conservation requires that the flow of charge corresponding to the pacing current also be accounted for, as failure to account for the pacing current induces a gradual drift in the variables. Following Hund et al. (18) we have assumed that this charge is carried by potassium ions.

Respiratory acidosis was simulated by increasing extracellular CO_2 from its control value of 5% with constant extracellular bicarbonate concentration. Extracellular pH is determined from the equilibrium of the CO_2 hydration reaction (see Eq. 10). Experimental studies typically induce respiratory acidosis using 15% (3,7) to 30% (2) extracellular CO_2, and so we have compared cellular responses at these two values. Most experimental studies consider the response to 3–10 min of respiratory acidosis, and so for the majority of our simulations we have imposed the rise in extracellular CO_2 for a 5-min duration.

RESULTS

To study the effects of each of the pH sensitivities described above, the pH-dependent rate laws were included in the model one at a time (using rate laws at normal pH value for each of the other mechanisms). In these initial simulations we wish to distinguish between the effects of pH on Ca^{2+}-handling mechanisms and direct effects of the pH regulatory processes, and therefore sarcolemmal proton transport fluxes (in particular NHE and NBC) are held at their normal (pH 7.15) values. In the absence of transmembrane acid fluxes, a step-increase in extracellular CO_2 from 5% control produces the pH profiles shown in Fig. 6. Fifteen-percent CO_2 produces a drop to pH 6.9 and 30% to ~6.7. These pH values compare well with experimental records of intracellular pH with 15% CO_2, for which Harrison et al. (7) measured intracellular pH fall to ~6.9, and 30% CO_2, for which Orchard and Kentish (2) estimated an intracellular pH drop of ~0.4 units.

Effects of acidosis on SR calcium

To examine the direct effects of the pH-dependence on SR calcium, we simulated respiratory acidosis with sarcolemmal proton transport maintained at normal values, in order to compare model predictions to data collected in saponin-skinned trabeculae preparations by Kentish and Xiang (6).

Inhibition of SR Ca^{2+} release channels

Fig. 7 shows the effects on cytosolic Ca^{2+} and SR Ca^{2+} content ($[Ca^{2+}]_{sr}$) produced by inhibition of Ca^{2+} release, Eq. 1, during acidosis. Fig. 7, *a–d*, shows $[Ca^{2+}]_i$ and $[Ca^{2+}]_{sr}$ with increasing acid load, indicating that, despite a reduction of the open probability to ~35% of its norm-acidic value as pH approaches 6.5, there is only a relatively minor decrease in peak systolic Ca^{2+}, with a small increase in diastolic Ca^{2+}. The figure shows an initial decrease in peak Ca^{2+} at the onset of acidosis (60 s) which rapidly recovers to near-normal levels, despite the sustained low pH, due to loading of the SR with Ca^{2+}. On the release of acidosis after 5 min, peak Ca^{2+} rises initially but rapidly returns to normal level. By contrast, the SR Ca^{2+} load rises when pH starts to fall, and the increased SR load is sustained during the period of acidosis. Thus inhibition of the SR release channels appears to have only a transient effect on cytosolic Ca^{2+}. SR Ca^{2+} content increases, which closely compensates for the reduced open probability of the release channels.

TABLE 3 Kinetic parameter values for the sarcolemmal acid transporters

Parameter	Units	NBC	NHE	CHE	AE
k_1^+	ms^{-1}	0.997×10^{-2}	0.121×10^{-1}	0.429×10^{-2}	0.352
k_1^-	ms^{-1}	0.560×10^{-1}	0.329×10^{-2}	0.250	0.347
k_2^+	ms^{-1}	0.853×10^{-4}	0.733×10^{-3}	0.681×10^{-1}	0.354
k_2^-	ms^{-1}	0.142×10^{-4}	0.269×10^{-2}	0.117×10^{-2}	0.360
K_{Na}	mM	0.487×10^4	0.336×10^2	—	—
K_{Cl}	mM	—	—	0.180×10^5	0.984×10^3
K_{HCO3}	mM	0.802×10^{-2}	—	—	0.111×10^3
pK_H	—	—	6.783	7.950	—
pK_i	—	6.738	6.464	—	7.573
n_i	—	2.91	3.18	—	5.11
pK_e	—	7.185	—	—	6.506
n_e	—	2.18	—	—	1.44

Note that, for CHE, we give the equivalent pK for OH^- transport as a proton dissociation constant: $pK_{OH} = 14 - pK_H$.

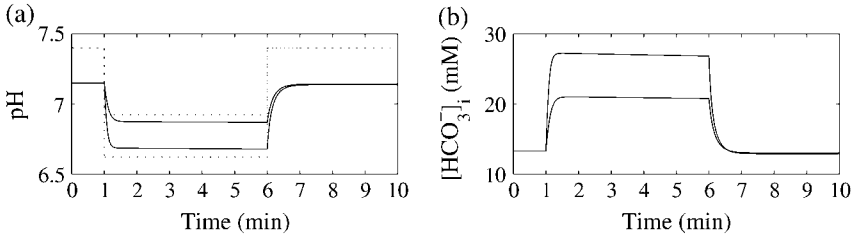

FIGURE 6 Effect of 15% and 30% extracellular CO_2 on intracellular pH (*a*) and HCO_3^- (*b*) in cell model with no pH sensitivity of the sarcolemmal proton transporters. Extracellular CO_2 is increased from 5% (control) to 15% or 30% after 1 min, and returned to control after 5 min of acidosis. Corresponding extracellular pH is also shown (*dotted*).

Normalized Ca^{2+} transients are shown in Fig. 7 *e*, showing that inhibition of Ca^{2+} release causes a slight but progressive delay in the time to peak, and has little effect on the rate of recovery of the Ca^{2+} transients.

Inhibition of SR Ca^{2+} uptake

In simulations for which the only pH-dependence included is inhibition of Ca^{2+} uptake into the SR, using Eq. 2, the opposite effect to inhibition of the release channels is seen. Peak systolic Ca^{2+} rises at the onset of acidosis, before recovery to normal levels, accompanied by a dramatic decrease in SR Ca^{2+} load, as shown in Fig. 8, *a–d*. After recovery from this initial spike in cytosolic Ca^{2+}, diastolic Ca^{2+} remains raised compared to normal, also recovering to control on release of the acidosis. These results show that in the absence of changes to sarcolemmal Ca^{2+} fluxes, the inhibition of SR Ca^{2+} uptake reduces SR Ca^{2+} content until near-normal cytosolic Ca^{2+} is achieved.

Inhibition of the SR Ca^{2+}-ATPase has a pronounced effect on the shape of individual Ca^{2+} transients, shown in Fig. 8 *e*, where time to peak is delayed (SR Ca^{2+} load is reduced and hence the Ca^{2+} release flux is lower) and recovery to (elevated) diastolic level is slowed, as would be expected as a direct result of slowed reuptake.

We performed simulations that combine inhibition of SR Ca^{2+} uptake and release to simulate experiments done by Kentish and Xiang (6) in permeabilized trabeculae. In these experiments the SR is loaded under constant intracellular Ca^{2+}, at different pH values. SR load was estimated by measuring the caffeine-induced Ca^{2+} release. The effect on the Ca^{2+} transient was measured by triggering Ca^{2+}-induced Ca^{2+} release from the SR using flash photolysis. We simulated the permeabilized membrane by uncoupling $[Ca^{2+}]_i$ from all sarcolemmal Ca^{2+} currents, and introducing a flux to maintain intracellular Ca^{2+},

$$J_{bal} = \frac{[Ca^{2+}]_e - [Ca^{2+}]_i}{\tau_{bal}}, \tag{20}$$

where we set the extracellular Ca^{2+} to be the steady-state resting intracellular calcium concentration $[Ca^{2+}]_e = 4.7 \times 10^{-5}$ mM, and the time constant for calcium transfer into the permeabilized cell, $\tau_{bal} = 18$ ms. To simulate the Kentish and Xiang experiments, we allowed the SR to load for 3 min, by which time a steady state was established, and then triggered Ca^{2+}-induced Ca^{2+} release using a calcium flux of 0.00015 mM/ms for 5 ms. Results for normalized SR load and $t_{1/2}$ for the decay of the calcium transient are shown in Fig. 9.

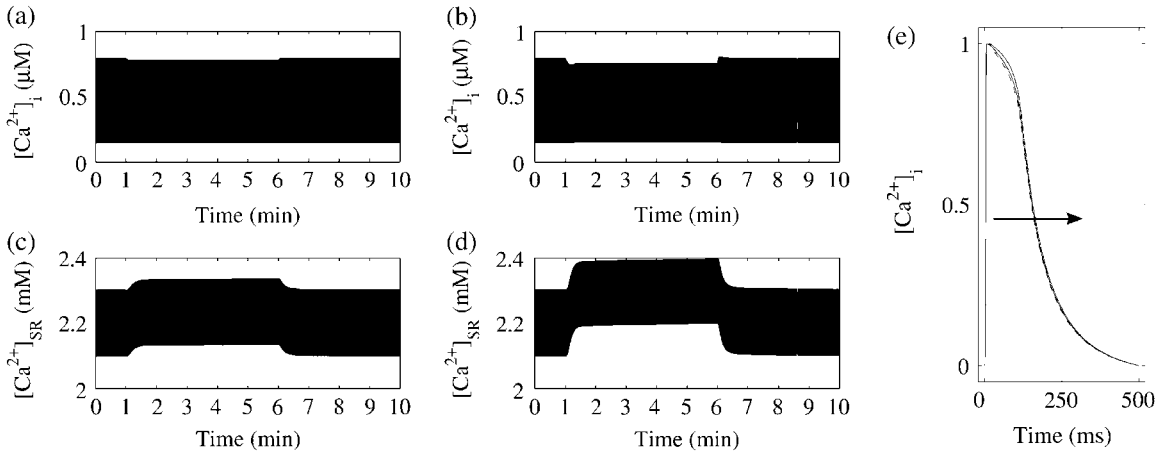

FIGURE 7 Effect of pH-dependent inhibition of RYRs on intracellular Ca^{2+} transient (*a* and *b*), and SR Ca^{2+} content (*c* and *d*), with 15% (*a* and *c*), and 30% (*b* and *d*), extracellular CO_2. SR Ca^{2+} content is calculated according to $[Ca]_{sr} = (V_{nsr}[Ca]_{nsr} + V_{jsr}[Ca]_{jsr})/V_{sr}$. (*e*) Intracellular Ca^{2+} transients (at 150 s, *solid lines*), with zeroed diastolic level and unit-normalized amplitude, allowing direct comparison of the recovery timescales with the normal transient (at 50 s, *dotted line*). Increasing CO_2 is indicated by the arrow.

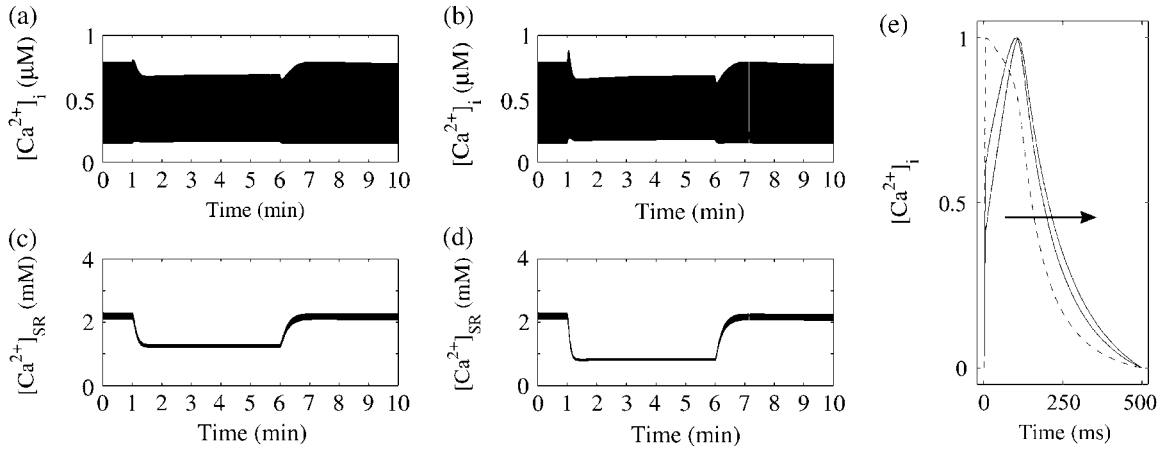

FIGURE 8 Effect of pH-dependent inhibition of SERCA on intracellular Ca^{2+} transients and SR Ca^{2+} content with 15% (*a* and *c*) and 30% CO_2 (*b* and *d*). Normalized intracellular Ca^{2+} transients are shown in *e*. Details as for Fig. 7.

Inhibition of sarcolemmal Ca^{2+} efflux

Inhibition of sarcolemmal Ca^{2+} efflux pathways also has a dramatic effect on SR Ca^{2+} load, which rises significantly during acidosis. Fig. 10, *c* and *d*, show the effect of the pH-sensitivity of the Na^+-Ca^{2+} exchange current described in Eq. 3. As total cell Ca^{2+} must rise with inhibition of net Ca^{2+} efflux from the cell, cytosolic Ca^{2+} rises, and the SR accumulates Ca^{2+} until efflux from the cell and influx via the L-type channels are again balanced during each cycle.

Although the rise in SR Ca^{2+} accompanying acidosis when NCX flux is inhibited is considerably higher than we found for RyR inhibition, we note that this rise is proportionately lower than the reduction in SR Ca^{2+} load due to inhibition of the SR Ca^{2+}-ATPase, as shown in Fig. 8. (We note, however, that Na^+ rises during acidosis, studied below, and so acidosis has a secondary influence on Ca^{2+} efflux by the exchanger through the direct effects of rising Na^+ on the exchanger flux.)

During acidosis, systolic Ca^{2+} is much higher than normal and the increase in peak Ca^{2+} is greater than the rise in diastolic Ca^{2+}; however, the effect on the normalized Ca^{2+} transients shown in Fig. 10 *e* is that recovery is slightly more rapid.

Competitive binding of protons at TnC Ca^{2+} sites

The effect of the pH-dependence for Ca^{2+} binding to Troponin-C was included using the pH-sensitive apparent binding coefficient, Eq. 7. Although TnC is one of the major buffers for Ca^{2+} in the cytosol, we found that competitive binding of protons to the low-affinity Ca^{2+} binding sites has minimal effect on the Ca^{2+} transient profile, shown in Fig. 11 *e*, and has much less pronounced effects on intracellular Ca^{2+} during acidosis, Fig. 11, *a–d*, although this is still highly important for excitation-contraction coupling due to the modified Ca^{2+}-tension curve, as shown in Fig. 4. As would be expected for a reduction in buffering power, competitive binding at the Ca^{2+} sites raises systolic Ca^{2+} and lowers diastolic Ca^{2+} (showing that the cell is less able to resist changes in Ca^{2+} due to reduced buffering).

Na^+ loading during acidosis

In the acidotic myocyte, the individual effects described above in response to a fall in pH occur against a background of pH regulation by the sarcolemmal acid and acid-equivalent transporters. Simulation of the effects of transmembrane acid transport on intracellular Na^+ and its knock-on effects on Ca^{2+} were performed by including the pH-sensitivity of the transporter fluxes in Eqs. 16–19. The change in intracellular pH after a step increase in extracellular CO_2 from 5% to 15% or 30% is shown in Fig. 12 *a*, and the corresponding intracellular HCO_3^- in Fig. 12 *b*. This figure, contrasted to Fig. 6, shows the biphasic nature of pH change during respiratory acidosis arising from a step change in

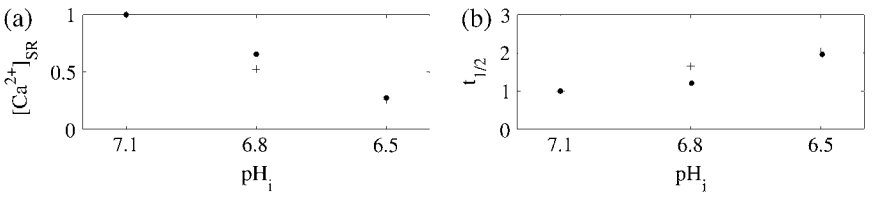

FIGURE 9 Normalized SR Ca^{2+} load (*a*) and $t_{1/2}$ for fall of Ca^{2+} transient (*b*) in permeabilized myocytes as a function of pH. (●) Experimental data from Kentish and Xiang (6) and (+) simulation results. SR Ca^{2+} load is measured after loading for 3 min at resting Ca^{2+} concentration, $t_{1/2}$ is measured for the Ca^{2+} transient after CICR. As Kentish and Xiang did not directly measure SR calcium load, we have assumed that releasable SR calcium concentration is proportional to the initial increase in $[Ca^{2+}]_i$ on application of caffeine, calculated from peak $[Ca^{2+}]_i$ and $t_{1/2}$ for rise, from Kentish and Xiang (their Fig. 3 *B*).

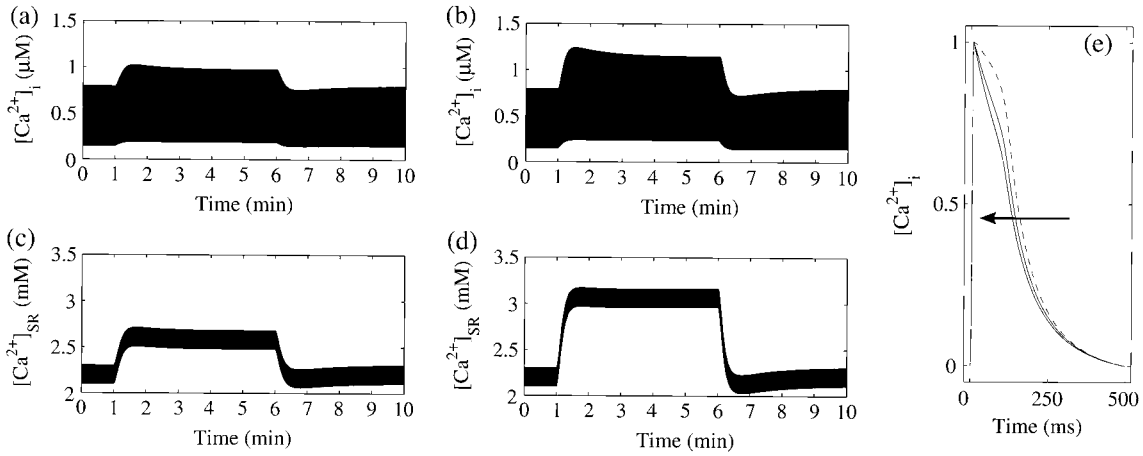

FIGURE 10 Effect of pH-dependent inhibition of NCX on Ca^{2+} transients and SR Ca^{2+} content with 15% (*a* and *c*) and 30% CO_2 (*b* and *d*). Normalized intracellular Ca^{2+} transients are shown in *e*. Details as for Fig. 7.

extracellular CO_2, with a rapid decline in pH_i followed by a slower partial recovery. This slow recovery of intracellular pH toward control level is due to sarcolemmal transport of protons and bicarbonate.

While the transporter fluxes have a direct effect on the pH, and therefore on the responses described above, acid efflux also produces a concomitant increase of intracellular sodium both by the Na^+-H^+ exchanger, which brings in one Na^+ for each H^+ exported, and by the Na^+-HCO_3^- cotransporter, which imports one Na^+ for each HCO_3^- brought into the cell. The increase in intracellular Na^+ corresponding to a step increase in extracellular CO_2 is shown in Fig. 12 *c* (*dotted lines*). As is shown in the figure, this increase in $[Na^+]_i$ can be very significant. The change in intracellular Na^+ therefore generates a secondary effect of acidosis on NCX, as Ca^{2+} efflux is less favored due to reduced gradient of Na^+ across the sarcolemma.

Na^+ influx coupled to H^+ efflux, in addition to the Na^+ that comes into the cell during the upstroke of the action potential, must be removed from the cytosol. Increasing Na^+ upregulates the Na^+-pump, which transports 3 Na^+ out of the cell and 2 K^+ in to the cell. Thus, the increased Na^+ efflux is coupled to an increased K^+ influx, raising intracellular K^+ as shown (*dotted lines*) in Fig. 12 *d*. When extracellular CO_2 is stepped back to control, pH quickly recovers and in fact overshoots control pH to more alkaline levels in each case. As pH recovers, acid efflux, and hence coupled Na^+ influx, falls and $[Na^+]_i$ starts to recover. Intracellular K^+ continues to rise, however, as the accumulated Na^+ is removed by the Na^+-pump. $[K^+]_i$ starts to fall only after Na^+ has recovered to near-control levels. It is worthy of note that the removal of extracellular CO_2 produces an overshoot in pH to more alkaline values, shown in Fig. 12 *a*, via the loading mechanism proposed by Boron and Weer (33). High membrane permeability to CO_2 means this removal quickly produces an equivalent drop in intracellular CO_2 which shifts the equilibrium of Eq. 11 to the left. Membrane impermeable bicarbonate ions that have

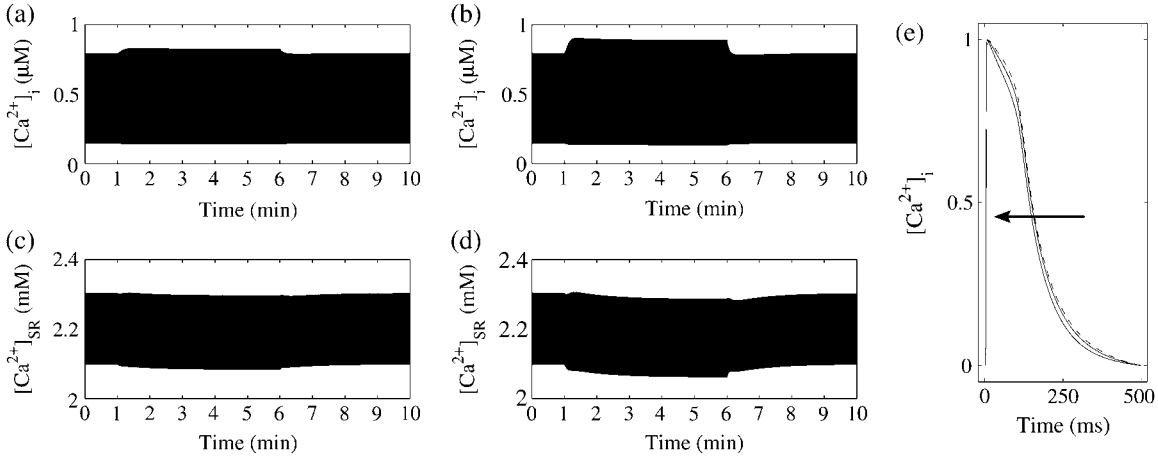

FIGURE 11 Effect of pH-dependent reduced affinity of Ca^{2+} binding to TnC on intracellular Ca^{2+} transients and SR Ca^{2+} content with 15% (*a* and *c*) and 30% CO_2 (*b* and *d*) Normalized intracellular Ca^{2+} transients are shown in *e*. Details as for Fig. 7.

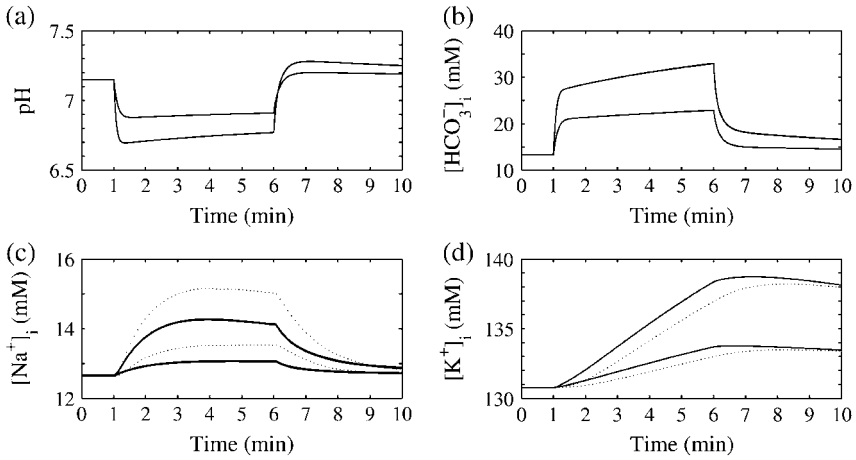

FIGURE 12 Effect of respiratory acidosis on intracellular pH (*a*), $[HCO_3^-]$ (*b*), $[Na^+]$ (*c*), and $[K^+]$ (*d*). Extracellular CO_2 is increased from 5% (control) to 15% and 30% at 1 min, and returned to control after 5 min of acidosis. The results of two independent simulations are shown: incorporating sarcolemmal pH transporters with no other pH-dependent changes (*dotted lines*), and the full dynamic model (*solid lines*). pH and HCO_3^- curves are indistinguishable for these two simulations.

been transported into the cell by NBC during acidosis now bind to protons producing the increase in pH.

The effects of rising intracellular Na^+ on intracellular Ca^{2+} are shown in Fig. 13. For these simulations the rising Na^+ is the only directly induced effect. These simulations show that reduced Ca^{2+} efflux on NCX due to rising Na^+ leads to an increase of systolic Ca^{2+} and a slight rise of diastolic Ca^{2+}, accompanied by rising SR Ca^{2+} load.

Excitation-contraction coupling in the full model of acidosis

The net effects of acidosis on Ca^{2+} transients and tension due to the combined actions of each of these pH-dependent processes are shown in Fig. 14, and corresponding pH, HCO_3^-, Na^+, and K^+ traces are shown in Fig. 12 (*solid lines*).

These simulations show a significant rise in diastolic Ca^{2+} at the onset of acidosis. From the results presented above, this is the combined effect of direct inhibition of NCX and SERCA. Systolic Ca^{2+} also rises, although this is much more evident for 30% CO_2 (Fig. 14 *b*). After the initial rise in systolic Ca^{2+} there is also a secondary increase before systolic Ca^{2+} starts to recover toward normal levels. This slower rise appears to be due to the accumulation of Na^+, which is an indirect mechanism by which acidosis reduces Ca^{2+} efflux on NCX. Another effect of this slow pH recovery is the slow fall of diastolic Ca^{2+} after the initial phase, which is due to the reduction in the level of inhibition of SERCA as pH rises, combined with the reduced efflux of Ca^{2+} caused by the accumulation of Na^+. For mild acidosis, Fig. 14 *a*, intracellular Ca^{2+} returns to normal directly on removal of respiratory acidosis. For acidosis with 30% CO_2, Fig. 14 *b*, there is a significant Ca^{2+} rebound subsequent to the return of CO_2 to control.

The Ca^{2+} rebound after the return to control CO_2 is somewhat paradoxical, given that, in these simulations, the total intracellular Ca^{2+} content (which is dominated by SR Ca^{2+}) actually falls during acidosis (Fig. 14, *c* and *d*). The cause of the overload is the slow reaccumulation of Ca^{2+} during acidosis, which is shown by rising SR Ca^{2+} in Fig.

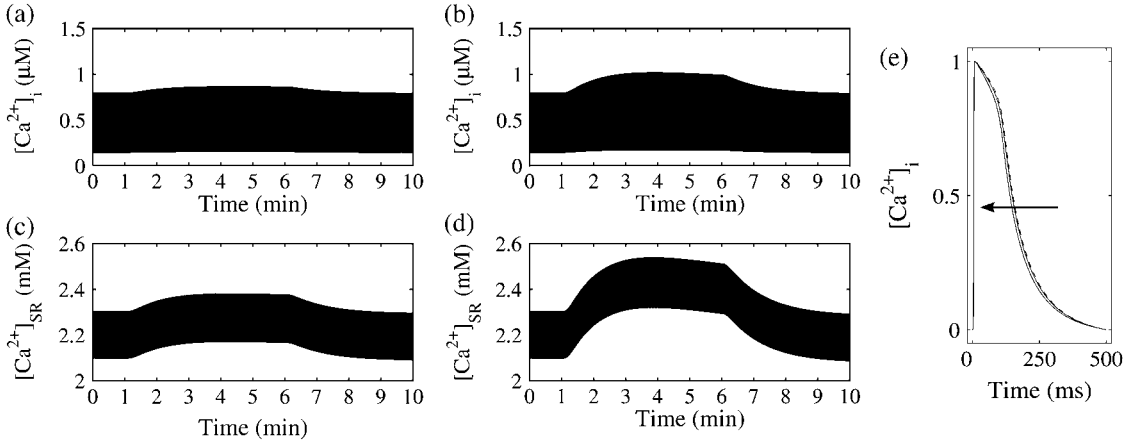

FIGURE 13 Effects of sarcolemmal acid-equivalent transport (and consequent Na^+ influx) on intracellular Ca^{2+} transients and SR Ca^{2+} content with 15% (*a* and *c*) and 30% CO_2 (*b* and *d*). Normalized intracellular Ca^{2+} transients are shown in *e*. Details as for Fig. 7.

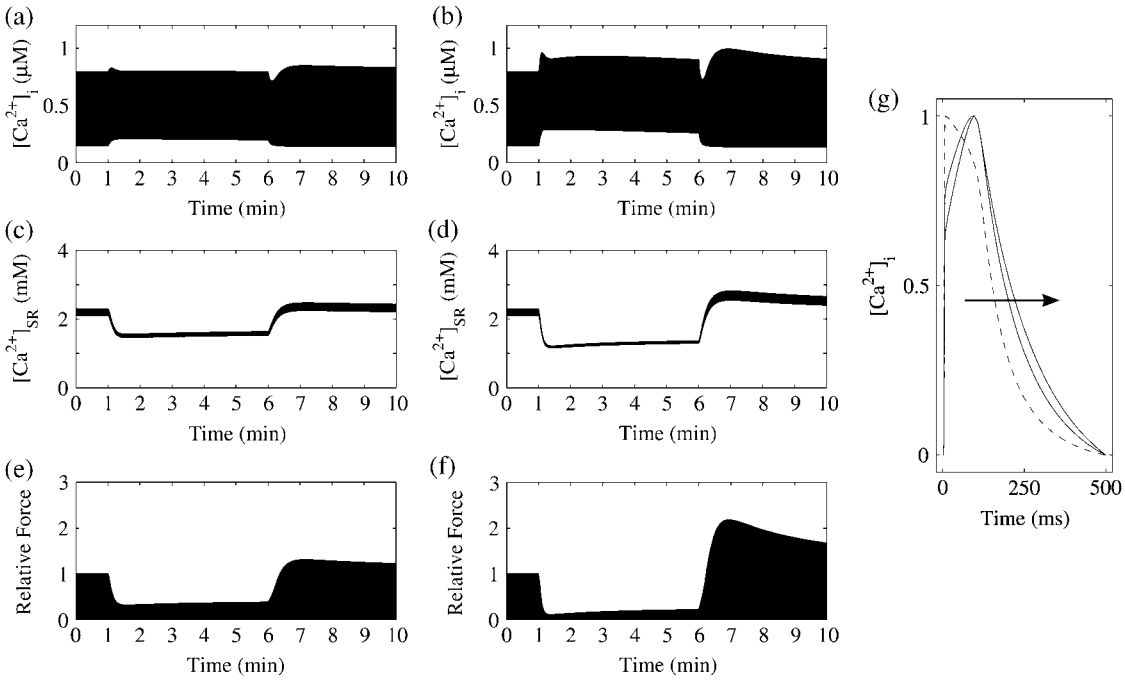

FIGURE 14 Effects of acidosis on Ca^{2+} transients, SR Ca^{2+} content, and tension in the full dynamic model with 15% (*a*, *c*, and *e*) and 30% CO_2 (*b*, *d*, and *f*). Normalized intracellular Ca^{2+} transients are shown in *g*. Details as for Fig. 7.

14 *d*. This gradual loading of the cell, due to the secondary reduction of Ca^{2+} efflux as Na^+ accumulates, means that the cell has a higher Ca^{2+} content just before release of inhibition, at the return of CO_2 to control, than it did after the initial rapid change in Ca^{2+} at the onset of acidosis. Furthermore, recovery from the overload to control Ca^{2+} levels after release of acidosis takes longer than would normally be the case, because this extra Ca^{2+} must be removed while Na^+ is still elevated. This mechanism suggests that the Ca^{2+} rebound will be greater if acidosis is maintained for a longer period (giving more time for Ca^{2+} accumulation), and this predicted increase is demonstrated in Fig. 15, in which acidosis is maintained for 10 min, twice as long as in the previous simulations.

The rapid drop in tension at the onset of acidosis reflects the initial drop in pH, Fig. 14, *e* and *f*. Slower partial recovery of tension during acidosis suggests recovery is due directly to the recovery of pH in the biphasic pH change. Tension also shows a significant overshoot after removal of the extracellular CO_2 load, which is more pronounced at 30% CO_2. There are two potential factors underlying this tension-increase overshoot: the Ca^{2+} overload after return of CO_2 to control, Fig. 14 *b*, and the pH overshoot evident in Fig. 12 *a*. For acidosis with 30% CO_2, the maximal tension transients occur some 60 s after the return of external CO_2 to normal, Fig. 14 *f*. By contrast, the pH reaches a maximum of pH 7.28 after ~50 s, remaining at this elevated level for several minutes, Fig. 12 *a*, while systolic Ca^{2+} peaks 45 s after return to the control CO_2 level, Fig. 14 *b*. The timings of these maxima therefore suggest that both Ca^{2+} and pH play a role. In the simulations, intracellular Ca^{2+} is always well below saturating concentration for the Troponin-C binding sites, even during the Ca^{2+} overload. From the Ca^{2+}-tension relationship, plotted at different pH in Fig. 4, increasing trigger Ca^{2+} from 0.8 μM (normal) to 1.5 μM at normal pH raises tension by a factor of ~1.75, while tension transients triggered by normal Ca^{2+} at pH 7.28 are ~1.35 times stronger. These effects combine to give the ~2.2-fold increase in the magnitude of tension transients seen in Fig. 14 *f*.

DISCUSSION

Our modeling study enables us to dissect the effects of acidosis on excitation-contraction coupling, as well as the role of the pH-regulatory mechanisms in the cell. It is noteworthy that for each of the pH-response curves with which we have characterized the pH-dependence of the steps in excitation-contraction coupling, normal intracellular pH is on the steep part, where the sensitivity to pH changes is highest. This is an additional indication that the myocyte is highly sensitive to pH, in addition to the finding by Leem et al. (35) that the sarcolemmal proton transporters under normal conditions operate in a permissive range, in which all transporters are active at low levels to set the normal steady-state pH.

Excitation-contraction coupling during acidosis

The simulations suggest that the most significant sustained effects on cytosolic Ca^{2+} during acidosis are due to elevated

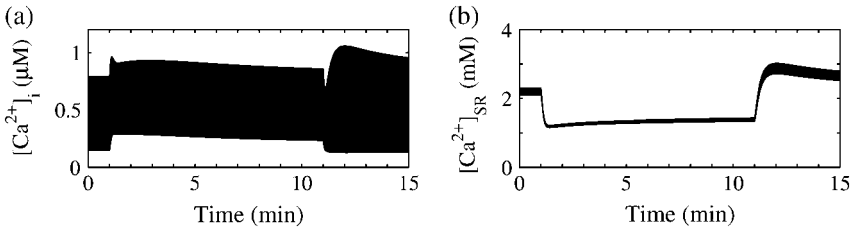

FIGURE 15 The effect of a longer period of acidosis on Ca^{2+} transients (*a*) and SR Ca^{2+} content (*b*) with 30% CO_2. Extracellular CO_2 is increased from 5% (control) to 30% after 1 min, and returned to control after 10 min of acidosis.

$[Na^+]_i$ and pH-dependent inhibition of NCX, both contributing to rising diastolic and peak systolic Ca^{2+}. Some earlier experimental studies reported no change or even reduced cytosolic Ca^{2+} levels at low pH. From our simulations, the only mechanism that contributes a reduction of cytosolic Ca^{2+} is inhibition of the sarcoplasmic reticulum Ca^{2+} release channels (RyRs), and this gave only a transient drop in systolic Ca^{2+} levels. Each of the other acidotic changes increases cytosolic Ca^{2+}. This response to RyR inhibition appears to be consistent with the data from Choi et al. (5), who reported a drop in cytosolic Ca^{2+} during acidosis. They observed that the recovery to control levels of cytosolic Ca^{2+}, after an immediate decrease at the onset of acidosis, was accompanied by an increase in SR load in voltage-clamped rat ventricular myocytes with inhibited sarcolemmal proton transporters (NHE and NBC). Similarly, when pH was returned to normal, systolic Ca^{2+} increased and subsequently recovered to control as the SR load returned to normal.

Given the significance of elevated $[Na^+]_i$, it may be important to note that recent experimental evidence (45) questions the previously accepted 1:1 electroneutral stoichiometry for Guinea-pig myocytes (35), as assumed in our model. This in turn has important implications for the relative activities of NBC and NHE. Specifically, if NBC imports more than one bicarbonate ion per sodium ion it will, in effect, be sodium-sparing relative to NHE. Another interesting finding is that the Na^+ influx on NHE during acidosis generates a greater influx of K^+ due to increased activity of the Na^+-pump. During ischemia this increased influx of K^+ might usefully act against the buildup of extracellular K^+ that is associated with arrhythmia.

SR Ca^{2+} load during acidosis

Our study indicates that the major influences on SR Ca^{2+} load during acidosis are inhibition of Ca^{2+} uptake and inhibition of NCX, which have opposing effects on SR calcium. Therefore, the overall effect on SR calcium observed in the whole cell (in the fully coupled model) during acidosis depends on the balance between mechanisms raising SR Ca^{2+} (reduction of Ca^{2+} efflux through the sarcolemma, such as NCX and to a lesser extent rising intracellular Na^+) and those reducing the Ca^{2+} load (primarily the inhibition of the SR Ca^{2+}-ATPase).

Reports on SR calcium content during acidosis in the literature are mixed. Kentish and Xiang (6), as well as several earlier reports, found that SR Ca^{2+} load decreases. Experiments on caffeine-induced calcium release from the SR at pH 6.5 showed that releasable SR Ca^{2+} was down to 40% of pH 7.1 levels. However, the majority of the other reports in the literature found that SR calcium content increases (7), but fractional release decreases during acidosis (4). It seems clear that these differences reflect the various experimental protocols and the conditions in which the measurements were made. One possibility is that experimental data obtained in nonphysiological conditions, such as in purified cell extracts, may not reflect the normal response of the intact cell, due to alterations to, or removal of, accessory or regulatory pathways in the cell. For example, although many studies have reported direct inhibition of the SR Ca^{2+}-pump at low pH or during acidosis (2,12,21,23), Choi et al. (5) inferred no significant change to SERCA flux from the lack of change to the rate of decline of individual Ca^{2+} transients. Thus one possible explanation for our finding that the experimentally reported level of inhibition of the SR calcium pump leads to a substantial decrease in SR Ca^{2+} in the whole-cell response, rather than the reported increase, is that these data do not include a compensatory mechanism by which the uptake by the pump is substantially maintained. In particular, the data we have used to parameterize the inhibition of Ca^{2+}-ATPase were measured in purified SR vesicles.

Several studies have found that CaMKII-related activation of SERCA may, at least partly, compensate for the direct inhibition of the pump by protons. Komukai et al. (29) showed that, in the presence of the CaMKII inhibitor KN-93, the caffeine-induced release of Ca^{2+} from the SR was lower than control during acidosis. The proposed mechanism is that elevated intracellular Ca^{2+} causes phosphorylation of the SR membrane-bound regulatory protein phospholamban by CaMKII, which enhances pump function (29,46). This could reconcile the disparate experimental data on SR Ca^{2+} load during acidosis, as is demonstrated by the model. In Fig. 16 the effects of acidosis with zero change to SR Ca^{2+} uptake are shown—the extreme case where there is no net effect on the SR Ca^{2+}-pump. In this case SR Ca^{2+} rises, as would be expected, consistent with current experimental findings. This is one possible explanation for the discrepancy, at least.

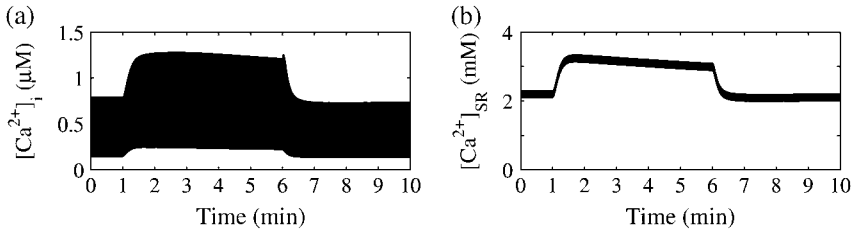

FIGURE 16 Acidosis without inhibition of SERCA: simulating effects of CaMKII on intracellular Ca^{2+} (*a*) and SR Ca^{2+} content (*b*) during respiratory acidosis with 30% CO_2. (See Fig. 14, *b* and *d*, for comparison.)

Another observation arising from this simulation is that when SR Ca^{2+} increases at the onset of acidosis, the slow recovery of pH due to net acid efflux from the cell causes a slow decline in the SR content, rather than the gradual increase that was observed when the SR content fell. In this case the release of acidosis at the return to control extracellular CO_2 level does not produce an overshoot in intracellular Ca^{2+}. This is consistent with the finding that it is the partial recovery of SR Ca^{2+} levels during acidosis that is responsible for the overshoot on the return to control CO_2. This suggestion, that intracellular Ca^{2+} overshoot on recovery is associated with falling SR content during acidosis, is a prediction of our model worth further experimental investigation.

Inhibition of sodium-hydrogen exchange during acidosis

Harrison et al. (7) found that the slow partial recovery of contractility was blocked when NHE (and hence Na^+ rise) was blocked by the selective NHE inhibitor amiloride. They also found that complete inhibition of SR release (by ryanodine) blocked the recovery of the twitch but did not affect the Na^+ rise. Thus we can infer that the effect of elevated Na^+ is mediated by increasing diastolic Ca^{2+}, consistent with the model results. Therefore the slow recovery of pH during prolonged acidosis contributes both a direct effect and an indirect effect, rising systolic Ca^{2+}, which is a consequence of pH regulatory mechanisms. Both mechanisms act to recover tension.

To get a biphasic response to respiratory acidosis, there must be processes occurring on (at least) two distinct timescales underlying the fast initial drop and the slower partial recovery of the contractile twitches. In our model, underlying the slow recovery, which increases the calcium transient and contributes to the recovery of the twitch during acidosis, is the slow recovery of intracellular pH itself, even as the imposed CO_2 is held at constant level. If NHE is blocked, the model predicts that the slow recovery of pH is abolished, and with it the rise in Na^+, as illustrated in Fig. 17. In fact, blocking NHE produced a slight decrease in intracellular Na^+, as shown in the figure, due in particular to reduced influx on NCX.

Other reports have implicated an alternative mechanism which may contribute to the slow recovery of tension. Nomura et al. (47) found, during prolonged acidosis, that the recovery of twitch contractions was at least partly due to CaMKII-dependent stimulation of SR Ca^{2+} uptake, and was abolished by the selective CaMKII inhibitor KN-93, although they found that the increase in $[Ca^{2+}]_i$ was not the sole mechanism for the recovery of contraction. DeSantiago et al. (46) also found that the slow recovery was abolished by KN-93, and was absent in phospholamban-knockout mice. As mentioned above, this CaMKII and time-dependent aspect of SR Ca^{2+} uptake is not represented in our model, and may contribute a further mechanism for the slower recovery phase of the cellular response to acidosis.

A further observation from this simulation is that blocking NHE, which produced a slight decrease in intracellular Na^+, also abolished the Ca^{2+} overload on removal of acidosis, consistent with our hypothesis that it is due to the slow recovery. This is a significant observation in relation to the so-called pH paradox in ischemia/reperfusion injury (48), in which cell injury is worsened after reperfusion when pH returns to normal levels after prolonged acidosis. The simulation results show that our model supports the view that cell injury (in this case Ca^{2+} overload and contracture) may be prevented by inhibition of sarcolemmal NHE flux, despite the abolition of the pH recovery, and shows that the mechanism of this injury is the slow accumulation of Ca^{2+} in the cell, which is avoided by preventing the rise in intracellular Na^+.

One of the strongest motives for studying the effects of acidosis in cardiac myocytes is that in ischemic myocardium the intracellular pH can fall to ~6.8 in the first 2 min of ischemia, and to ~6.5 after 5 min (49,50), and may ultimately fall by as much as one pH unit (51). During ischemia, there are several other pH-dependent mechanisms, as well as many pH-independent processes that alter cell function and viability. One important consideration for acidosis during ischemia (rather than respiratory acidosis) is that intracellular proton buffering by inorganic phosphate (Pi), which is negligible under normal conditions, may become significant as Pi rises strongly in the ischemic myocyte. The changes in proton generation in the cell, due to the change in metabolism, as well as proton-coupled transport of lactate and pyruvate, must be considered. These effects have not been considered here. Additionally, there are many other significant cellular changes during ischemia that impact on cellular Ca^{2+} handling mechanisms and excitation-contraction coupling.

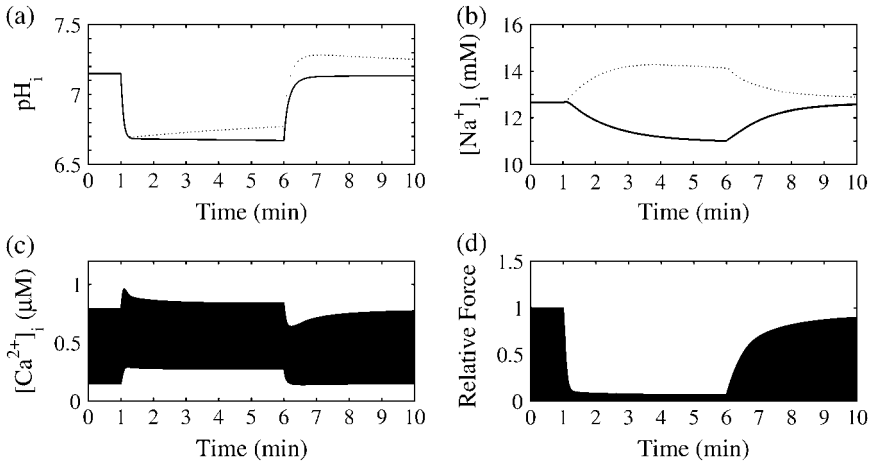

FIGURE 17 Effects of NHE block (amiloride) on slow recovery of pH (*a*), $[Na^+]_i$, (*b*), $[Ca^{2+}]_i$ (*c*), and tension (*d*) during acidosis with 30% CO_2. The gradual pH recovery and increasing $[Na^+]_i$ in the full cell model are shown for comparison (*dotted line*). (See Fig. 14, *b* and *f*, for comparison of $[Ca^{2+}]_i$ and tension profiles.)

Some of these are considered in an earlier simulation of pH regulation in myocardial ischemia by Ch'en et al. (52).

The simulations of acidosis we have presented show that, in our model, the acidosis-related changes in the cell are reversible. On return to normal pH, the excitation-contraction coupling and force generation also return to normal values, as is observed in experimental studies of respiratory acidosis. Changes to cell function and injury arising during ischemia and reperfusion are, of course, not reversible. Our study thus supports the view that the irreversible damage to the ischemic heart is not due directly to acidosis, but may be due to the underlying depletion of metabolic intermediates and to accumulation of products in poorly perfused tissue.

There are also potentially highly significant spatial effects of acidosis which we have not incorporated in this model: both intracellular pH localization and mobility (53,54), and effects between cells including gap junctional permeability and pH gradients across cardiac tissue, which have been recorded in multicellular preparations (55,56). We are currently extending our model to include such spatial effects, as well as other changes that occur during ischemia, to predict the effects of localized loss of perfusion on whole-heart function.

APPENDIX

Assuming a constant extracellular ionic environment, cell membrane potential E_m (mV) is determined from charge balance considerations (44) (also called the ''algebraic method'' (18)),

$$E_m(t) = \frac{FV_{myo}}{C_m A_m}\left(\sum_X z_X [X]_i(t) + \gamma\right),$$
$$X = Na^+, K^+, Ca^{2+}, H^+, Cl^-, HCO_3^-, \qquad (21)$$

where A_m (cm^2) is the capacitative cell membrane area, V_{myo} (μL) is the available cell volume, C_m ($\mu F\ cm^{-2}$) is the capacitance per unit area of the membrane, and F is Faraday's constant. The constant γ is determined by the initial (resting) values for the transmembrane potential and intracellular concentrations, and represents the contribution from all intracellular impermeant charged species and the initial charge separation across the membrane. The value $[X]_i$ represents the total (buffered and free) cellular concentrations (mM) of each ionic species in the model, with valences of z_X; for example, the total calcium concentration is determined from

$$[Ca^{2+}]_{tot} = [Ca^{2+}]_i + [Ca^{2+}]_{trpn} + [Ca^{2+}]_{cmdn} + \frac{V_{nsr}}{V_{myo}}[Ca^{2+}]_{nsr} + \frac{V_{jsr}}{V_{myo}}([Ca^{2+}]_{jsr} + [Ca^{2+}]_{csqn}). \qquad (22)$$

Because this calculation requires buffered Ca^{2+} concentrations, these are calculated explicitly (see the Supplementary Material for further details).

While chloride ions are not accounted for in the LRd model, a chloride current must be included in this formulation to balance the influx of chloride ions on the acid transporters AE and CHE (described below), for Eq. 21 to be valid. Therefore we include a constant-field sarcolemmal chloride current, specifically

$$I_{Cl} = p_{Cl}\frac{F^2 E_m}{RT}\left(\frac{[Cl^-]_i - [Cl^-]_e e^{FE_m/RT}}{1 - e^{FE_m/RT}}\right), \qquad (23)$$

where the membrane permeability $p_{Cl} = 1.0 \times 10^{-7}$ cm ms^{-1} and extracellular chloride concentration is held constant at $[Cl^-]_e = 126$ mM (43), and the intracellular chloride concentration is determined by

$$\frac{d[Cl^-]_i}{dt} = \frac{A_m I_{Cl}}{F V_{myo}} + J_{che} + J_{ae}. \qquad (24)$$

Inclusion of the sarcolemmal transporters NHE and NBC into the model contribute an additional Na^+ influx under normal pH conditions. Hence we have adjusted the background Na^+ current to $g_{Na,b} = 0.002\ \mu A\ \mu F^{-1}$ to give the same resting Na^+ flux, and increased the maximal Na-pump current to maintain a steady intracellular sodium concentration $\overline{I_{NaK}} = 3.0\ \mu A\ \mu F^{-1}$.

Acid-equivalent transporters

We describe the acid-equivalent transporters using simplified flux expressions for compulsory order sequential cotransport and exchange. Detailed balance at thermodynamic equilibrium for the transport cycle imposes a constraint on the transition rates. Under the assumption that ion association and dissociation reactions from the protein are rapid, this constraint is given by

$$k_1^+ k_2^+ = k_1^- k_2^-, \qquad (25)$$

where $k_1^\pm$ and $k_2^\pm$ are forward and backward rates for transitions between the two conformations of the transporters. This rapid equilibrium assumption for ion binding allows the kinetic description of the six-state cycles to be reduced to an equivalent two-state scheme, where the state transition rates depend on the intra- and extracellular ligand concentrations. For a compulsory-order cotransporter, these transition rates are given by

$$\alpha_1^+ = \frac{k_1^+ K_A K_B}{K_A K_B + K_B[A]_i + [A]_i[B]_i}$$
$$\alpha_1^- = \frac{k_1^- K_A K_B}{K_A K_B + K_B[A]_e + [A]_e[B]_e}$$
$$\alpha_2^+ = \frac{k_2^+ [A]_e[B]_e}{K_A K_B + K_B[A]_e + [A]_e[B]_e}$$
$$\alpha_2^- = \frac{k_2^- [A]_i[B]_i}{K_A K_B + K_B[A]_i + [A]_i[B]_i},$$

and the steady-state transport flux for the cotransporter is

$$J_{\text{cotrans}}(A,B) = \frac{\alpha_1^+ \alpha_2^+ - \alpha_1^- \alpha_2^-}{\alpha_1^+ + \alpha_1^- + \alpha_2^+ + \alpha_2^-}. \quad (26)$$

Similarly, the six-state compulsory order exchanger flux can be reduced to an equivalent two-state cycle using the rapid equilibrium assumption with state transition rates:

$$\beta_1^+ = \frac{k_1^+ K_B[A]_i}{K_A K_B + K_B[A]_i + K_A[B]_i}$$
$$\beta_1^- = \frac{k_1^- K_B[A]_e}{K_A K_B + K_B[A]_e + K_A[B]_e}$$
$$\beta_2^+ = \frac{k_2^+ K_A[B]_e}{K_A K_B + K_B[A]_e + K_A[B]_e}$$
$$\beta_2^- = \frac{k_1^- K_A[B]_i}{K_A K_B + K_B[A]_i + K_A[B]_i}.$$

The steady-state exchanger flux J_{exch} is given by

$$J_{\text{exch}}(A,B) = \frac{\beta_1^+ \beta_2^+ - \beta_1^- \beta_2^-}{\beta_1^+ + \beta_1^- + \beta_2^+ + \beta_2^-}. \quad (27)$$

A full derivation of these fluxes is given in the Supplementary Material.

SUPPLEMENTARY MATERIAL

An online supplement to this article can be found by visiting BJ Online at http://www.biophysj.org. The model described in this work is available from the authors as a FORTRAN program.

Both authors thank Dr. Peter Mulquiney, Professors Richard Vaughan-Jones and Clive Orchard, Dr. Denis Loiselle, and the Ischaemia Discussion Group at the Bioengineering Institute, Auckland, for helpful discussions.

E.J.C. and N.P.S. are supported by the Marsden Fund of the Royal Society of New Zealand through grant No. 04-UOA-177 and National Institutes of Health grant No. EB005825, and E.J.C. acknowledges support from the Wellcome Trust, London, and the New Zealand Institute for Mathematics and Its Applications for part of this work.

REFERENCES

1. Bers, D. M., and D. Ellis. 1982. Intracellular calcium and sodium activity in sheep heart Purkinje fibres: effect of changes of external sodium and intracellular pH. *Pflugers Arch.* 393:171–178.
2. Orchard, C. H., and J. C. Kentish. 1990. Effects of changes of pH on the contractile function of cardiac muscle. *Am. J. Physiol.* 258:C967–C981.
3. Allen, D. G., and C. H. Orchard. 1983. The effects of changes of pH on intracellular calcium transients in mammalian cardiac muscle. *J. Physiol.* 335:555–567.
4. Hulme, J. T., and C. H. Orchard. 1998. Effect of acidosis on Ca^{2+} uptake and release by sarcoplasmic reticulum of intact rat ventricular myocytes. *Am. J. Physiol.* 275:H977–H987.
5. Choi, H. S., A. W. Trafford, C. H. Orchard, and D. A. Eisner. 2000. The effect of acidosis on systolic Ca^{2+} and sarcoplasmic reticulum calcium content in isolated rat ventricular myocytes. *J. Physiol.* 529:661–668.
6. Kentish, J., and J.-Z. Xiang. 1997. Ca^{2+}- and caffeine-induced Ca^{2+} release from the sarcoplasmic reticulum in rat skinned trabeculae: effects of pH and P_i. *Cardiovasc. Res.* 33:314–323.
7. Harrison, S. M., J. E. Frampton, E. McCall, M. R. Boyett, and C. H. Orchard. 1992. Contraction and intracellular Ca^{2+}, Na^+, and H^+ during acidosis in rat ventricular myocytes. *Am. J. Physiol.* 262:C348–C357.
8. Wakabayashi, S., and K. Goshima. 1981. Kinetic studies on sodium-dependent calcium uptake by myocardial cells and neuroblastoma cells in culture. *Biochim. Biophys. Acta.* 642:158–172.
9. Philipson, K. D., M. M. Bersohn, and A. Y. Nishimoto. 1982. Effects of pH on Na^+-Ca^{2+} exchange in canine cardiac sarcolemmal vesicles. *Circ. Res.* 50:287–293.
10. Doering, A. E., and W. J. Lederer. 1993. The mechanism by which cytoplasmic protons inhibit the sodium-calcium exchanger in Guinea-pig heart cells. *J. Physiol.* 466:481–499.
11. Bountra, C., and R. D. Vaughan-Jones. 1989. Effect of intracellular and extracellular pH on contraction in isolated, mammalian cardiac muscle. *J. Physiol.* 418:163–187.
12. Fabiato, A., and F. Fabiato. 1978. Effects of pH on the myofilaments and the sarcoplasmic reticulum of skinned cells from cardiac and skeletal muscle. *J. Physiol.* 276:233–255.
13. Blanchard, E. M., and R. J. Solaro. 1984. Inhibition of the activation and troponin calcium binding of dog cardiac myofibrils by acidic pH. *Circ. Res.* 55:382–391.
14. Faber, G. M., and Y. Rudy. 2000. Action potential and contractility changes in $[Na^+]_i$ overloaded cardiac myocytes: a simulation study. *Biophys. J.* 78:2392–2404.
15. Hunter, P. J., A. D. McCulloch, and H. E. D. J. ter Keurs. 1998. Modelling the mechanical properties of cardiac muscle. *Prog. Biophys. Mol. Biol.* 69:289–331.
16. Crampin, E. J., N. P. Smith, A. E. Langham, R. H. Clayton, and C. H. Orchard. 2006. Acidosis in models of cardiac ventricular myocytes. *Philos. Trans. R. Soc. A.* In press.
17. Luo, C. H., and Y. Rudy. 1994. A dynamic model of the cardiac ventricular action potential. I. Simulations of ionic currents and concentration changes. *Circ. Res.* 74:1071–1096.
18. Hund, T. J., J. P. Kucera, N. F. Otani, and Y. Rudy. 2001. Ionic charge conservation and long-term steady state in the Luo-Rudy dynamic cell model. *Biophys. J.* 81:3324–3331.
19. Rousseau, E., and J. Pinkos. 1990. pH modulates conducting and gating behaviour of single calcium release channels. *Eur. J. Physiol.* 415:645–647.
20. Xu, L., G. Mann, and G. Meissner. 1996. Regulation of cardiac Ca^{2+} release channel (ryanodine receptor) by Ca^{2+}, H^+, Mg^{2+} and adenine nucleotides under normal and simulated ischemic conditions. *Circ. Res.* 79:1100–1109.
21. Mandel, F., E. G. Kranias, A. G. D. Gende, M. Sumida, and A. Schwartz. 1982. The effect of pH on the transient-state kinetics of Ca^{2+}-Mg^{2+}-ATPase of cardiac sarcoplasmic reticulum. A comparison with skeletal sarcoplasmic reticulum. *Circ. Res.* 50:310–317.
22. Martonosi, A. 1969. Sarcoplasmic reticulum. VII. Properties of a phosphoprotein intermediate implicated in calcium transport. *J. Biol. Chem.* 244:613–620.
23. Shigekawa, M., J.-A. M. Finegan, and A. M. Katz. 1976. Calcium transport ATPase of canine cardiac sarcoplasmic reticulum: a comparison with that of rabbit fast skeletal muscle sarcoplasmic reticulum. *J. Biol. Chem.* 251:6894–6900.

24. Khan, Y. M., J. M. East, and A. G. Lee. 1997. Effects of pH on phosphorylation of the Ca^{2+}-ATPase of sarcoplasmic reticulum by inorganic phosphate. *Biochem. J.* 321:671–676.
25. Henderson, I. M. J., Y. M. Khan, J. M. East, and A. G. Lee. 1994. Binding of Ca^{2+} to the (Ca^{2+}-Mg^{2+})-ATPase of sarcoplasmic reticulum: equilibrium studies. *Biochem. J.* 297:615–624.
26. Pick, U., and S. J. D. Karlish. 1982. Regulation of the conformational transition in the Ca-ATPase from sarcoplasmic reticulum by pH, temperature, and calcium ions. *J. Biol. Chem.* 257:6120–6126.
27. Doering, A. E., and W. J. Lederer. 1994. The action of Na^+ as a cofactor in the inhibition by cytoplasmic protons of the cardiac Na^+-Ca^{2+} exchanger in the Guinea-pig. *J. Physiol.* 480:9–20.
28. Egger, M., and E. Niggli. 2000. Paradoxical block of the Na^+-Ca^{2+} exchanger by extracellular protons in Guinea-pig ventricular myocytes. *J. Physiol.* 523:353–366.
29. Komukai, K., C. Pascarel, and C. H. Orchard. 2001. Compensatory role of CaMKII on I_{Ca} and SR function during acidosis in rat ventricular myocytes. *Pflugers Arch.* 442:353–361.
30. Marban, E., and H. Kusuoka. 1987. Maximal Ca^{2+}-activated force and myofilament Ca^{2+} sensitivity in intact mammalian hearts. *J. Gen. Physiol.* 90:609–623.
31. Komukai, K., T. Ishikawa, and S. Kurihara. 1989. Effects of acidosis on Ca^{2+} sensitivity of contractile elements in intact ferret myocardium. *Am. J. Physiol.* 274:H147–H154.
32. Li, G., A. F. Martin, and J. R. Solaro. 2001. Localization of regions of Troponin I important in deactivation of cardiac myofilaments by acidic pH. *J. Mol. Cell. Cardiol.* 33:1309–1320.
33. Boron, W. F., and P. D. Weer. 1976. Intracellular pH transients in squid giant axons caused by CO_2, NH_3, and metabolic inhibitors. *J. Gen. Physiol.* 67:91–112.
34. Leem, C. H., and R. D. Vaughan-Jones. 1998. Out-of-equilibrium pH transients in the Guinea-pig ventricular myocyte. *J. Physiol.* 509:471–485.
35. Leem, C. H., D. Lagadic-Gossmann, and R. D. Vaughan-Jones. 1999. Characterization of intracellular pH regulation in the Guinea-pig ventricular myocyte. *J. Physiol.* 517:159–180.
36. Smith, N. P., and E. J. Crampin. 2004. Development of models of active ion transport for whole-cell modelling: cardiac sodium-potassium pump as a case study. *Prog. Biophys. Mol. Biol.* 85:387–405.
37. Lagadic-Gossmann, D., K. J. Buckler, and R. D. Vaughan-Jones. 1992. Role of bicarbonate in pH recovery from intracellular acidosis in the Guinea-pig ventricular myocyte. *J. Physiol.* 458:361–384.
38. Vaughan-Jones, R. D., and K. W. Spitzer. 2002. Role of bicarbonate in the regulation of intracellular pH in the mammalian ventricular myocyte. *Biochem. Cell Biol.* 80:579–596.
39. Ch'en, F. F.-T., and R. D. Vaughan-Jones. 2001. $Na^+ - HCO_3^-$ cotransport is instructed by pH and not bicarbonate or Na^+. *Biophys. J.* 80:74a.
40. van Borren, M. M., A. Baartscheer, R. Wilders, and J. H. Ravesloot. 2004. NHE-1 and NBC during pseudo-ischemia/reperfusion in rabbit ventricular myocytes. *J. Mol. Cell. Cardiol.* 37:567–577.
41. Gill, P. E., W. Murray, M. A. Saunders, and M. H. Wright. 1984. Procedures for optimization problems with a mixture of bounds and general linear constraints. *ACM Trans. Math. Softw.* 10:282–298.
42. Sun, B., C. H. Leem, and R. D. Vaughan-Jones. 1996. Novel chloride-dependent acid loader in the Guinea-pig ventricular myocyte: part of a dual acid-loading mechanism. *J. Physiol.* 495:65–82.
43. Vaughan-Jones, R. D. 1986. An investigation of chloride-bicarbonate exchange in the sheep cardiac Purkinje fibre. *J. Physiol.* 379:377–406.
44. Grabe, M., and G. Oster. 2001. Regulation of organelle acidity. *J. Gen. Physiol.* 117:329–343.
45. Yamamoto, T., P. Swietach, A. Rossini, S. H. Loh, R. Vaughan-Jones, and K. W. Spitzer. 2004. Functional diversity of electrogenic $Na^+ - HCO_3^-$ co-transport in ventricular myocytes from rat, rabbit and Guinea pig. *J. Physiol.* 562:455–475.
46. DeSantiago, J., L. S. Maier, and D. M. Bers. 2004. Phospholamban is required for CaMKII-dependent recovery of Ca transients and SR Ca reuptake during acidosis in cardiac myocytes. *J. Mol. Cell. Cardiol.* 36:67–74.
47. Nomura, N., H. Satoh, H. Terada, M. Matsunaga, H. Watanabe, and H. Hayashi. 2002. CaMKII-dependent reactivation of SR Ca^{2+} uptake and contractile recovery during intracellular acidosis. *Am. J. Physiol.* 283:H193–H203.
48. Bond, J. M., E. Chacon, B. Herman, and J. J. Lemasters. 1993. Intracellular pH and Ca^{2+} homeostasis in the pH paradox of reperfusion injury to neonatal rat cardiac myocytes. *Am. J. Physiol.* 265:C129–C137.
49. Garlick, P. B., G. K. Radda, and P. J. Seeley. 1979. Studies of acidosis in the ischaemic heart by phosphorus nuclear magnetic resonance. *Biochem. J.* 184:547–554.
50. Mohabir, R., H. Lee, R. W. Kurz, and W. Y. Clusin. 1991. Effects of ischemia and hyperbaric acidosis on myocyte calcium transients, contraction and pH_i in perfused rabbit hearts. *Circ. Res.* 69:1525–1537.
51. Bak, M. I., and J. S. Ingwall. 1994. Acidosis during ischemia promotes adenosine-triphosphate resynthesis in postischemic rat-heart: in-vivo regulation of 5′-nucleotidase. *J. Clin. Invest.* 93:40–49.
52. Ch'en, F. F.-T., R. D. Vaughan-Jones, K. Clarke, and D. Noble. 1998. Modelling myocardial ischaemia and reperfusion. *Prog. Biophys. Mol. Biol.* 69:515–538.
53. Vaughan-Jones, R. D., B. E. Peercy, J. P. Keener, and K. W. Spitzer. 2002. Intrinsic H^+ ion mobility in the mammalian ventricular myocyte. *J. Physiol.* 541:139–158.
54. Zaniboni, M., P. Swietach, A. Rossini, T. Yamamoto, K. W. Spitzer, and R. D. Vaughan-Jones. 2003. Intracellular proton mobility and buffering power in cardiac ventricular myocytes from rat, rabbit and Guinea pig. *Am. J. Physiol.* 285:H1236–H1246.
55. Zaniboni, M., A. Rossini, P. Swietach, N. Banger, K. W. Spitzer, and R. D. Vaughan-Jones. 2003. Proton permeation through the myocardial gap junction. *Circ. Res.* 93:726–735.
56. Swietach, P., K. W. Spitzer, and R. D. Vaughan-Jones. 2005. Experimental generation and computational modeling of intracellular pH gradients in cardiac myocytes. *Biophys. J.* 88:3018–3037.
57. Orchard, C. H., S. R. Houser, A. A. Kort, A. Bahinski, M. C. Capogrossi, and E. G. Lakatta. 1987. Acidosis facilitates spontaneous sarcoplasmic reticulum Ca^{2+} release in rat myocardium. *J. Gen. Physiol.* 90:145–165.